Available online at www.sciencedirect.com
ScienceDirect
Geochimica et Cosmochimica Acta 74 (2010) 6157–6173
Geochimica et Cosmochimica Acta
www.elsevier.com/locate/gca

"Invisible" silver and gold in supergene digenite ($Cu_{1.8}S$)

Martin Reich [a,*], Stephen L. Chryssoulis [b], Artur Deditius [c], Carlos Palacios [a], Alejandro Zúñiga [d], Magdalena Weldt [a], Macarena Alvear [a]

[a] Departamento de Geología, Facultad de Ciencias Físicas y Matemáticas, Universidad de Chile, Santiago, Chile
[b] Advanced Mineral Technology Laboratory (AMTEL), London, Ontario, Canada
[c] Institute of Applied Geosciences, Graz University of Technology, Graz, Austria
[d] Departamento de Ingeniería Mecánica, Facultad de Ciencias Físicas y Matemáticas, Universidad de Chile, Santiago, Chile

Received 12 April 2010; accepted in revised form 27 July 2010; available online 4 August 2010

Abstract

Despite its potential economic and environmental importance, the study of trace metals in supergene (secondary) Cu-sulfides has been seriously overlooked in the past decades. In this study, the concentration and mineralogical form of "invisible" precious metals (Ag, Au) and metalloids (As, Sb, Se, Te) in supergene digenite ($Cu_{1.8}S$) from various Cu deposits in the Atacama Desert of northern Chile, the world's premier Cu province, were determined in detail using a combination of micro-analytical techniques. Secondary ion mass spectrometry (SIMS) and electron microprobe analyzer (EMPA) measurements reveal that, apart from hosting up to ~11,000 ppm Ag, supergene digenite can incorporate up to part-per-million contents of Au (~6 ppm) and associated metalloids such as As (~300 ppm), Sb (~60 ppm), Se (~96 ppm) and Te (~18 ppm). SIMS analyses of trace metals show that Ag and Au concentrations strongly correlate with As in supergene digenite, defining wedge-shaped zones in Ag–As and Au–As log–log spaces. SIMS depth profiling and high-resolution transmission electron microscopy (HRTEM) observations reveal that samples with anomalously high Ag/As (>~30) and Au/As (>~0.03) ratios plot above the wedge zones and contain nanoparticles of metallic Ag and Au, while samples with lower ratios contain Ag and Au that is structurally bound to the Cu-sulfide matrix. The Ag–Au–As relations reported in this study strongly suggest that the incorporation of precious metals in Cu-sulfides formed under supergene, low-temperature conditions respond to the incorporation of a minor component, in this case As. Therefore, As might play a significant role by increasing the solubility of Ag and Au in supergene digenite and controlling the formation and occurrence of Ag and Au nanoparticles. Considering the fact that processes of supergene enrichment in Cu deposits can be active from tens of millions of years (e.g. Atacama Desert), we conclude that supergene digenite may play a previously unforeseen role in scavenging precious metals from undersaturated (or locally slightly supersaturated) solutions in near-surface environments.

1. INTRODUCTION

Supergene copper ores have received significant attention due to their global economic importance and the dramatic extent to which copper and sulfur are remobilized and fractionated during oxidative weathering (Brimhall et al., 1985; Ague and Brimhall, 1989; Lichtner and Biino, 1992; Mathur et al., 2005; Sillitoe, 2005; Belogub et al., 2008; Reich et al., 2009a). In addition to the economic upgrading of copper, resulting from weathering and re-precipitation of copper minerals, supergene enrichment processes have also been identified to cause strong enrichment in trace metals contents, most importantly nickel, cobalt, gold, silver and platinum-group elements. This (Ni, Co) has been reported in laterite deposits, while silver and gold are known to accumulate in supergene profiles from arid regions (Golightly, 1981; Bowles, 1986; Freyssinet et al., 1989; Boyle, 1997; Colin et al., 1997; Hough et al., 2008; Reich et al., 2009b). In addition, supergene processes

* Corresponding author. Tel.: +56 2 9784986
E-mail address: mreich@ing.uchile.cl (M. Reich).

0016-7037/$ - see front matter © 2010 Elsevier Ltd. All rights reserved.
doi:10.1016/j.gca.2010.07.026

in sulfidic ore systems can also contribute acid rock drainage and heavy metal leaching from the sulfides, resulting in natural contamination of the local environment and their adjacent surroundings (Martycak et al., 1994; Kimball et al., 1995; Hochella et al., 1999; Matlock et al., 2002).

Copper sulfides are widespread in both hypogene and supergene Cu deposits worldwide and are considered profitable Cu ores because of their high Cu-content at ~67–80 wt% Cu (Vaughan and Craig, 1978). Anilite ($Cu_{1.76}S$), digenite ($Cu_{1.8}S$), djurleite ($Cu_{1.97}S$) and chalcocite (Cu_2S) are the Cu-rich members of a group of minerals that range in composition from CuS (covellite) to Cu_2S (chalcocite) (Skinner, 1966; Morimoto and Koto, 1970; Morimoto and Gyobu, 1971; Will et al., 2002; Fleet, 2006). Despite their simple compositions, these Cu-sulfides are structurally complex and commonly can consist of multi-mineral mixtures at the micro and nanoscales (Posfai and Buseck, 1994; Makovicky, 2006).

Unlike hypogene Cu-sulfides, formed under magmato-hydrothermal conditions or during breakdown of high-temperature bornite (Cu_5FeS_4), secondary or supergene Cu-sulfides form when the Cu ore system is exposed at or near the surface and acidic and oxidizing solutions dissolve primary Cu-sulfides such as chalcopyrite and bornite. The breakdown of chalcopyrite, $CuFeS_2$ (Eq. (1)) produces soluble Cu ions that percolate downwards in the soil/regolith profile and precipitate below the water table or redox front to form, e.g. chalcocite, Cu_2S, under reducing conditions in the presence of bacteria (Sillitoe et al., 1996; Southam and Saunders, 2005; Enders et al., 2006; Kimball et al., 2009) (Eq. (2)):

$$CuFeS_2 + 16Fe^{3+} + 8H_2O = Cu^{2+} + 17Fe^{2+} + 2SO_4^{2-} + 16H^+ \quad (1)$$

$$2Cu^{2+} + HS^- = Cu_2S + H^+ \quad (2)$$

Among supergene Cu-sulfides, the Cu-rich members of this group (i.e. anilite, digenite, djurleite and chalcocite) are the most abundant and widely distributed secondary Cu-sulfides in ore systems, including porphyry Cu, stratabound "Manto-type" Cu, red-bed "Kupferschiefer" Cu and volcanic hosted massive sulfide (VHMS) Cu deposits (Large et al., 1995; Maksaev et al., 2007; Belogub et al., 2008; Reich et al., 2009b), and are also found as a secondary product of hypogene sulfide alteration in submarine magmatic–hydrothermal systems in mid-ocean ridges (Hannington et al., 1988; De Ronde et al., 2005).

Despite its economic and environmental importance, very few studies have documented the trace element content of supergene Cu-sulfides and Cu-sulfides in general. Among those studies, Hannington et al. (1988) reported secondary enrichment of Au and Ag in recent submarine sulfides in the TAG hydrothermal field in the Mid-Atlantic Ridge, containing up to 16 ppm Au as free native Au and 116 ppm Ag in Cu-sulfides. In a more recent study, Mozgova et al. (2008) documented up to 1200 ppm Ag and 1000 ppm Au in Cu-sulfides from the Ashadze hydrothermal field in the Mid-Atlantic.

In the Atacama Desert of northern Chile, which holds bout 40% of the known Cu resources in the world (Maksaev et al., 2007), significant amounts of "invisible" precious trace metals (Ag, Au) have been documented in Cu-sulfides from Cu deposits (Vivallo and Henriquez, 1998; Kojima et al., 2003; Reich et al., 2009b). For example, the high-grade, low-tonnage "Manto-type" Cu deposits of northern Chile host 8–25 g of Ag per ton (e.g. Mantos de la Luna, Susana/Lince and Buena Vista deposits, Kojima et al., 2003), and more than one million ounces of Ag have been produced as a by-product of the main Cu-sulfide mineralization at the Mantos Blancos deposit (Orrego et al., 2006). Weathering of the primary (hypogene) sulfide mineralization in these deposits produced several hundred meters of higher grade caps of secondary Cu-sulfides, oxides, hydroxides, carbonates, sulfates and chlorides. This supergene mineralization is a reflection of the history of groundwater flow, tectonics, landscape, and climate of the Atacama Desert (Alpers and Brimhall, 1988; Sillitoe and McKee, 1996; Clarke, 2006; Reich et al., 2009a).

Despite this evidence, the study of precious metal contents in supergene (secondary) Cu minerals has been largely overlooked in the past decades in Chile and elsewhere. In addition to the lack of trace-element data, thermodynamic and experimental studies of precious metal solubility (Ag, Au) in Cu-sulfides are available only at high temperatures, i.e. ~120–600 °C (Skinner, 1966; Ghosal and Sack, 1995; Sack, 2000; Fleet, 2006; Sack and Ebel, 2006). Under these magmato-hydrothermal temperature conditions, extensive solid solution has been documented in the Cu–Ag–S and Cu–Ag–Sb–As systems and results are only applicable to hydrothermal ore deposits where Ag is "visible" and form Ag sulfides and sulfosalts. Therefore, the solubility, speciation and mineralogical form of "invisible" precious metals in Cu-sulfides formed under non-equilibrium, low (<100 °C) temperature conditions in supergene environments remain unconstrained.

In this study, we used secondary ion mass spectrometry (SIMS) and electron microprobe analyzer (EMPA) to fully characterize the trace metal content of Ag-bearing supergene digenite from four Cu deposits in the Atacama Desert of northern Chile. When coupled with high-resolution transmission electron microcopy (HRTEM) observations, the trace-element data show that the solubility of Ag and Au in supergene digenite is strongly dependent of the As content, as previously reported for Au in As-rich pyrite (Cook and Chryssoulis, 1990; Reich et al., 2005, and references therein). We then explored how this information can be used to better understand the role of supergene Cu-sulfides as potential sinks of significant amounts of precious metals in supergene profiles.

2. SAMPLES AND METHODS

2.1. Samples

Supergene Cu-sulfide samples were obtained from stratabound (Mantos de la Luna, Michilla), porphyry-type (Mantos Blancos) and giant porphyry Cu (Spence) deposits in the Atacama Desert of northern Chile. All the deposits sampled have well-developed supergene enrichment profiles overlying the hypogene Cu-sulfide zones. Recent and

detailed descriptions of the geology of these deposits are found in Kojima et al. (2003), Reich et al. (2009b) (Mantos de la Luna), Trista-Aguilera et al. (2006) (Michilla), Ramirez et al. (2006) (Mantos Blancos), and Cameron et al. (2007) (Spence). For details about the age and relation between supergene enrichment and climate in the hyper-arid Atacama of northern Chile, the reader is referred to Sillitoe et al. (1996), Arancibia et al. (2006), Cameron et al. (2008) and Reich et al. (2008, 2009a).

In these deposits, supergene Cu-sulfides (digenite, djurleite and covellite) occur as disseminated fine-grained aggregates and in veinlets replacing the hypogene assemblage (bornite and chalcopyrite), and are locally altered to the oxide alteration assemblage of atacamite and chrysocolla. No Ag-minerals occur in these deposits, with the exception of small amounts of native Ag at Susana–Lince and Mantos Blancos deposits (Kojima et al., 2003).

Considering its dominant modal abundance in the studied material (21 samples), supergene digenites were analyzed using a combination of electron microprobe analysis (EMPA), secondary ion mass spectrometry (SIMS) and high-resolution transmission electron microscopy (HRTEM). In these samples, only discrete, homogeneous digenite mineral grains with no visible exsolutions and/or zonations were analyzed. The integration of EMPA, SIMS and HRTEM techniques allowed a full characterization of digenites in term of their major components stoichiometry, trace element contents and crystal structure (see Section 3).

2.2. Electron microprobe analysis (EMPA)

Major and trace element compositions of supergene digenite grains were obtained by wavelength-dispersive spectrometry (WDS) using a Cameca SX-100 electron microprobe analyzer at the University of Michigan Electron Microbeam Analysis Laboratory (EMAL). Digenites were measured for Cu (Kα), S (Kα), Fe (Kα), Ag (Lα), Au (Mα), As (Lα), Sb (Lβ), Se (Lα), Te (Lα), V (Kα), Co (Kα), Ni (Kα), Zn (Kα), Cd (Lα), Sn (Lα), Bi (Mα) and Hg (Mα) using a 2 μm beam, at 20 kV accelerating voltage and 10–40 nA beam current, with 30 s peak counting times for Cu, Fe and S. Higher counting times of 50–60 s (As, Sb, Se), 80 s (Te) and 80–100 s (Ag, Au) were used to increase counting rates for the aforementioned elements (V, Co, Ni, Zn, Cd, Sn, Bi and Hg were not detected during the analyses). Detection limits were 100 ppm (Se), 150 ppm (V, Ni), 200 ppm (Fe, S, As, Sb, Te, Co, Zn), 300 ppm (Ag, Au), 400 ppm (Cu), 450 ppm (Sn), 600 ppm (Bi) and 700 ppm (Cd, Hg). The following mineral and synthetic metal standards used were Cu_2S (Cu), FeS_2 (Fe, S), FeAsS (As), Sb_2S_3 (Sb), Se^0 (Se), SbTe (Te), Ag^0 (Ag), and Au^0 (Au). No beam-induced damage was observed during digenite analysis.

2.3. Secondary ion mass spectrometry (SIMS)

SIMS is currently one of the most sensitive microbeam techniques available for detecting trace concentrations of Ag and Au (and other traces metals) in sulfide minerals (Chryssoulis et al., 1987, 2004; Cook and Chryssoulis, 1990; Arehart et al., 1993; Larocque et al., 1995a,b; Reich et al., 2005). Along with other modern microanalytical techniques such as laser-ablation inductively coupled plasma mass spectrometry (LA-ICP-MS) and proton induced X-ray emission (PIXE) spectrometry, SIMS techniques provide a combination of sub-ppm detection limits with sub-micron scale mineral inclusion detection capabilities.

Multi-element (Ag, Au, As, Sb, Se, Te) SIMS analyses of supergene digenite from Mantos de la Luna, Michilla, Mantos Blancos and Spence were performed at Advanced Mineral Technology Laboratories (AMTEL) in London, Ontario, using a Cameca IMS-3f ion microprobe. A 10 kV and 8 nA primary Cs^+ beam source was used for measurements, with a 4.5 kV accelerating voltage for the negative secondary ions. The analytical spot of the primary beam was 15 μm at 8–10 nA and the depth of analysis was between 0.8 and 2 μm. The ions (isotopes) analyzed were $^{107,109}Ag^-$, $^{197}Au^-$, $^{75}As^-$, $^{121,123}Sb^-$, $^{128,130}Te$ and $^{78,80}Se$. In addition, the following major constituent ions were monitored: $^{63}Cu^-$, $^{34}S^-$ and $^{56}Fe^-$. Molecular interferences were eliminated by 180 eV offset with the energy slit fully open. The minimum detection limits at 2σ of the background level were 1.4 ppm (Ag), 0.07 ppm (Au), 0.5 ppm (As), 0.88 ppm (Sb), 0.05 ppm (Se) and 0.07 ppm (Te). The mineral standards used were produced by implanting a known dosage of the element of interest into the same mineral matrix (digenite) using the Tandetron accelerator at the University of Western Ontario, Canada. The implant dosage varies from 5×10^{13} atoms/cm^2 for Au up to 5×10^{14} atoms/cm^2 for Ag, with a typical implantation energy of 1 MeV. In depth profiles, the minimum detectable size of sub-micron mineral inclusions was 100 nm at 5 s counting time.

2.4. High-resolution transmission electron microscopy (HRTEM)

Unlike EMPA or SIMS, TEM techniques allow near-atomic scale imaging capabilities, along with *in-situ* determination of crystal structure by using selected area electron diffraction (SAED) and/or by fast Fourier transformation (FFT) of high-resolution images, and a qualitative determination of major elemental distribution by means of energy dispersive X-ray spectrometry (EDS). Therefore, TEM observations can be used as a complementary tool to obtain highly magnified images and structural/chemical information of both the sulfide matrix and the contained mineral nanoparticles.

The observation of selected digenite samples was carried out using a FEI Tecnai F20 FEG TEM operated at 200 kV, equipped with an EDS detector (~0.5–1 wt% detection limit), at the Laboratorio de Microscopía Electrónica de Transmisión (LabMET), Universidad de Chile, Santiago, Chile. Digenite grains with anomalously Ag contents and evidence of nanoparticulate Ag as measured by EMPA and SIMS depth profiling were cut from epoxy polished mounts and mounted into 3 mm diameter copper TEM grids. Final thinning of the samples was performed by ion milling with a 4.0 keV Ar beam in a Gatan ion-milling system. Radiation damage or phase transformations were not observed during ion milling and TEM observation. Image

analysis, including Fast Fourier Transformation (FFT), was completed using Gatan Digital Micrograph 3.4.

3. RESULTS

3.1. Major and trace element contents of supergene digenite: EMPA and SIMS results

Representative electron microprobe analyses of supergene digenite from Cu deposits are reported in Table 1. Cu and S contents of digenite vary from 76.35 to 79.01 wt%, and 20.77 to 21.97 wt%, respectively. Iron was only measured in a few grain samples, with contents ranging from 200 ppm to 0.49 wt%. Cu-deficiency is observed in all Cu-sulfide point analyses ($n = 88$), with a mean of 1.82 atoms per formula unit of Cu per each S, $Cu_{1.82}S$, with a small standard deviation (0.02) (Fig. 1A). This homogeneous compositional range of Cu is typical of the digenite-type solid solution ($Cu_{1.8}S$) (Will et al., 2002).

EMPA analyses show that Ag contents range from a maximum of 1.16 wt% (11,600 ppm) to below the minimum detection limit values of 300 ppm (Table 1). Apart from Ag, only traces of Se (~100 ppm) and Te (~200 ppm) were detected by EMPA in some samples, while Au, Sb and As are

Table 1
Representative electron microprobe analyzer (EMPA) data (wt%) of argentiferous supergene digenite. b.d. = below detection. Detection limits (wt%) are shown below each element analyzed.

Sample	Cu (0.04)	Fe (0.02)	S (0.02)	As (0.02)	Sb (0.02)	Se (0.01)	Te (0.02)	Ag (0.03)	Au (0.03)	Total
cc ML-4	77.61	b.d.	21.59	b.d.	b.d.	b.d.	b.d.	b.d.	b.d.	99.32
cc ML-4	78.03	b.d.	21.37	b.d.	b.d.	b.d.	b.d.	b.d.	b.d.	99.52
cc ML-4	78.08	b.d.	21.64	b.d.	b.d.	b.d.	b.d.	b.d.	b.d.	99.80
cc ML-4	78.17	b.d.	21.29	b.d.	b.d.	b.d.	b.d.	b.d.	b.d.	99.59
cc ML-4	77.97	b.d.	21.58	b.d.	b.d.	b.d.	b.d.	b.d.	b.d.	99.64
cc ML-4	77.96	b.d.	21.55	b.d.	b.d.	b.d.	b.d.	b.d.	b.d.	99.63
cc ML-4	77.78	b.d.	21.39	b.d.	b.d.	b.d.	b.d.	b.d.	b.d.	99.31
cc ML-4	77.51	b.d.	21.48	b.d.	b.d.	b.d.	b.d.	b.d.	b.d.	99.09
cc ML-4	77.97	b.d.	21.63	b.d.	b.d.	b.d.	b.d.	b.d.	b.d.	99.76
cc SS-1	77.65	b.d.	21.40	b.d.	b.d.	b.d.	b.d.	b.d.	b.d.	99.13
cc SS-1	77.78	b.d.	21.15	b.d.	b.d.	b.d.	b.d.	b.d.	b.d.	99.02
cc SS-1	77.75	b.d.	21.10	b.d.	b.d.	b.d.	b.d.	b.d.	b.d.	98.99
cc SS-1	77.91	b.d.	21.24	b.d.	b.d.	b.d.	b.d.	b.d.	b.d.	99.25
cc SS-1	77.87	b.d.	21.32	b.d.	b.d.	0.01	b.d.	0.04	b.d.	99.30
cc SS-1	77.53	b.d.	21.07	b.d.	b.d.	b.d.	b.d.	b.d.	b.d.	98.71
cc SS-1	77.80	b.d.	21.28	b.d.	b.d.	b.d.	b.d.	b.d.	b.d.	99.17
cc SS-1	77.88	b.d.	21.08	b.d.	b.d.	0.01	b.d.	b.d.	b.d.	99.09
cc SS-1	77.55	b.d.	21.33	b.d.	b.d.	b.d.	0.02	b.d.	b.d.	98.96
cc MB-14	79.01	b.d.	21.43	b.d.	b.d.	b.d.	b.d.	b.d.	b.d.	100.46
cc MB-14	78.94	b.d.	21.21	b.d.	b.d.	b.d.	b.d.	b.d.	b.d.	100.17
cc MB-14	78.60	b.d.	21.36	b.d.	b.d.	b.d.	b.d.	b.d.	b.d.	100.00
cc MB-14	77.43	0.02	21.46	b.d.	b.d.	b.d.	b.d.	b.d.	b.d.	98.94
cc MB-14	78.37	b.d.	21.33	b.d.	b.d.	b.d.	b.d.	b.d.	b.d.	99.72
cc MB-14	78.80	b.d.	21.35	b.d.	b.d.	b.d.	b.d.	b.d.	b.d.	100.19
cc MB-14	77.60	b.d.	21.50	b.d.	b.d.	b.d.	b.d.	b.d.	b.d.	99.11
cc MB-14	77.61	b.d.	21.79	b.d.	b.d.	b.d.	b.d.	b.d.	b.d.	99.43
cc MB-14	77.62	b.d.	21.64	b.d.	b.d.	b.d.	b.d.	0.03	b.d.	99.30
cc MB-14	77.46	b.d.	21.59	b.d.	b.d.	b.d.	b.d.	b.d.	b.d.	99.11
cc MB-14	77.72	b.d.	21.85	b.d.	b.d.	b.d.	b.d.	0.03	b.d.	99.62
cc MB-14	77.56	b.d.	21.73	b.d.	b.d.	b.d.	b.d.	b.d.	b.d.	99.32
cc ML-1	77.00	b.d.	20.77	b.d.	b.d.	b.d.	b.d.	0.86	b.d.	98.64
cc ML-1	77.09	b.d.	20.99	b.d.	b.d.	b.d.	b.d.	1.05	b.d.	99.13
cc ML-1	77.74	b.d.	21.67	b.d.	b.d.	b.d.	b.d.	0.43	b.d.	99.85
cc ML-1	78.33	b.d.	21.74	b.d.	b.d.	b.d.	b.d.	0.15	b.d.	100.23
cc ML-1	76.35	b.d.	21.16	b.d.	b.d.	b.d.	b.d.	0.60	b.d.	98.11
cc ML-1	77.44	b.d.	21.72	b.d.	b.d.	b.d.	b.d.	0.21	b.d.	99.37
cc ML-1	78.47	b.d.	21.94	b.d.	b.d.	0.01	b.d.	0.04	b.d.	100.47
cc ML-1	77.60	b.d.	21.80	b.d.	b.d.	b.d.	b.d.	1.16	b.d.	100.57
cc ML-1	76.94	0.49	21.80	b.d.	b.d.	0.01	b.d.	0.21	b.d.	99.45
cc ML-1	78.35	0.06	21.75	b.d.	b.d.	b.d.	b.d.	b.d.	b.d.	100.18
cc ML-1	78.22	0.05	21.87	b.d.	b.d.	b.d.	b.d.	b.d.	b.d.	100.18
cc ML-1	78.53	0.04	21.97	b.d.	b.d.	b.d.	b.d.	b.d.	b.d.	100.55
cc ML-1	78.36	b.d.	21.67	b.d.	b.d.	b.d.	b.d.	0.05	b.d.	100.09
cc ML-1	77.36	b.d.	21.57	b.d.	b.d.	b.d.	b.d.	0.08	b.d.	99.03
cc ML-4	77.61	b.d.	21.59	b.d.	b.d.	b.d.	b.d.	b.d.	b.d.	99.32

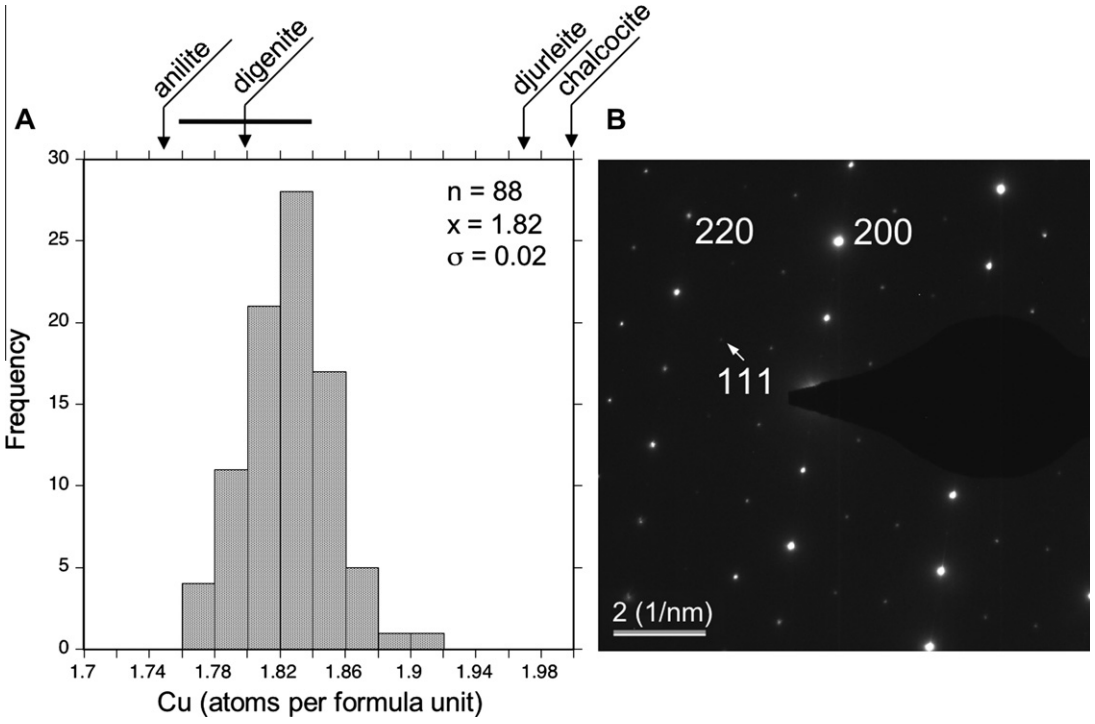

Fig. 1. Composition and structure of supergene Cu-sulfide samples analyzed in this study. (A) Histogram showing the compositional range of digenite, as measured by EMPA. The average formulae of 88 representative point analyses ($Cu_{1.82 \pm 0.02}S$) fall within the range of digenite-type solid solution series (horizontal line, Will et al., 2002). Also, the chemical formulae of anilite, djurleite and chalcocite, with respect to Cu-content, are shown above the upper scale (arrows). (B) TEM selected area electron diffraction (SAED) pattern of a representative digenite sample. Indexing of the two-dimensional lattice fringes reveals a cubic structure with space group *Fd3m* and $a = 5.57$ Å (low-digenite structure, Will et al., 2002).

below detection in most analyses (<200–300 ppm). No exsolved phases, chemical heterogeneities, zonations and/or growth zones were detected during EMPA (backscattered electron imaging mode, BSE) observation of digenite.

Because of its high accuracy and sub-ppm sensitivity, the SIMS method allowed the detection of trace elements (Ag, Au, As, Sb, Se, Te) that are present in digenite samples, and that are rarely reported in any microanalytical dataset. A summary of maximum, minimum and average concentrations of 259 SIMS analyses is presented in Table 2. Individual spot analyses are presented in Appendix A. Concentrations of Ag range from a maximum of ~3000 ppm to a minimum detected of ~1.5 ppm, and Au ranges between a maximum of ~6 ppm and a minimum of 0.07 ppm (70 ppb). Arsenic and antimony were detected in most samples, with maximum concentrations of ~300 and 60 ppm, respectively, and minimum contents of 0.5 and ~1 ppm, respectively. Concentrations of Se range between 96 and ~2 ppm, whereas Te

Table 2
Summary statistics of secondary ion mass spectrometry (SIMS) analyses (see Appendix A) of argentiferous digenite from various deposits in northern Chile. Mean concentrations ($\langle X \rangle$) are reported along with standard errors (σ).

Deposit	Datapoints		Ag [ppm]	Au [ppm]	As [ppm]	Sb [ppm]	Se [ppm]	Te [ppm]
Mantos de la Luna	96	max.	2977.00	5.98	277.00	51.40	91.30	17.90
		min.	1.77	0.07	0.5	0.95	1.82	0.63
		$\langle X \rangle \pm \sigma$	118.22 ± 36.36	0.65 ± 0.09	20.23 ± 4.40	6.93 ± 0.94	24.74 ± 2.42	6.90 ± 0.52
Michilla	101	max.	1346.00	3.12	189.00	59.50	96.00	16.70
		min.	1.77	0.07	0.5	1.17	2.53	0.58
		$\langle X \rangle \pm \sigma$	88.60 ± 18.59	0.51 ± 0.05	13.45 ± 3.07	8.37 ± 1.08	23.10 ± 2.13	6.58 ± 0.48
Mantos Blancos	37	max.	369.00	1.92	55.30	6.20	17.60	6.41
		min.	1.45	0.07	0.5	1.09	2.79	0.63
		$\langle X \rangle \pm \sigma$	54.13 ± 12.30	0.32 ± 0.08	5.75 ± 1.86	0.70 ± 0.26	10.02 ± 0.52	2.10 ± 0.17
Spence	25	max.	21.90	1.49	37.50	5.36	16.60	7.59
		min.	1.70	0.07	0.78	1.02	5.15	1.66
		$\langle X \rangle \pm \sigma$	8.03 ± 1.05	0.47 ± 0.07	6.76 ± 2.08	0.75 ± 0.27	7.88 ± 0.60	2.51 ± 0.25

concentrations vary from a maximum of ~18 ppm to a minimum of ~0.6 ppm.

Elemental correlation plots for SIMS analyses of trace metals in supergene digenite are shown in Fig. 2. When plotted in log–log space, Ag and Au show well-defined positive correlation trends with As (Fig. 2A and B, respectively), and with each other (Fig. 2C). In both cases (Ag *vs.* As and Au *vs.* As), the datapoints fall within wedge-shaped zones similar to the one reported for Au *vs.* As in arsenian pyrite by Reich et al. (2005). Insets in Fig. 2A–C show that Ag and Au also correlate with As, and with each other, in individual grains from representative samples. Another element that appears to positively correlate with Ag and Au is Sb, although the trends are more scattered (Fig. 2D and E). Antimony and As do not show an evident trend of correlation (Fig. 2F), although in some individual samples a positive correlation was observed (inset, Fig. 2F). Silver and Au do not correlate with Se or Te (not shown).

3.2. Mineralogical form of trace metals: SIMS depth profiles and TEM observations

The submicroscopic occurrence of "invisible" Ag (and Au) and associated trace metals in digenite was studied by using a combination of SIMS depth profiling and TEM observations. Two types of samples were selected based on the SIMS compositional data: (i) individual grain samples that show a positive correlation between Ag (and Au) *vs.* As, and that plot within the "wedge" (Fig. 2A), and (ii) individual samples with no visible correlation between Ag (and Au) *vs.* As that plot above the "wedge".

The dynamic mode of the SIMS analysis, whereby successively deeper layers of the mineral are analyzed with time, enables the distinction between solid-solution incorporation (homogeneous signal as a function of depth) and the occurrence of sub-micron, nanoscale inclusions from the sudden change in the element signal intensity between layers (Chryssoulis, 1990). The SIMS profiles for trace metals in selected digenite samples are presented in Fig. 3A–F. Depth-concentration profiles (time *vs.* intensity in counts per second) are presented for the digenite matrix isotopes (^{63}Cu, ^{34}S) and the contained trace elements (^{107,109}Ag, ^{75}As, ^{197}Au, ^{78,80}Se, ^{121,123}Sb and ^{128,130}Te). Along with Cu and S, the distribution of As, Se and Te is constant with depth, indicating that these elements are incorporated in solid solution in the digenite structure (Fig. 3C, D and F, respectively). Silver shows two mineralogical forms in digenite: nanoparticulate (Fig. 3A) and solid solution (Fig. 3B). The well-defined Ag spike in Fig. 3A suggest the presence of a Ag inclusion ~200 nm wide or a cluster of Ag nanoparticles smaller than 100 nm each. Gold and Sb profiles are spiky due to their low concentrations (Fig. 3D and E, respectively), and solid-solution incorporation is assumed.

The SIMS depth profiles do not provide information about the texture and crystal structure of the detected Ag sub-micron particles, and do not allow resolving individual

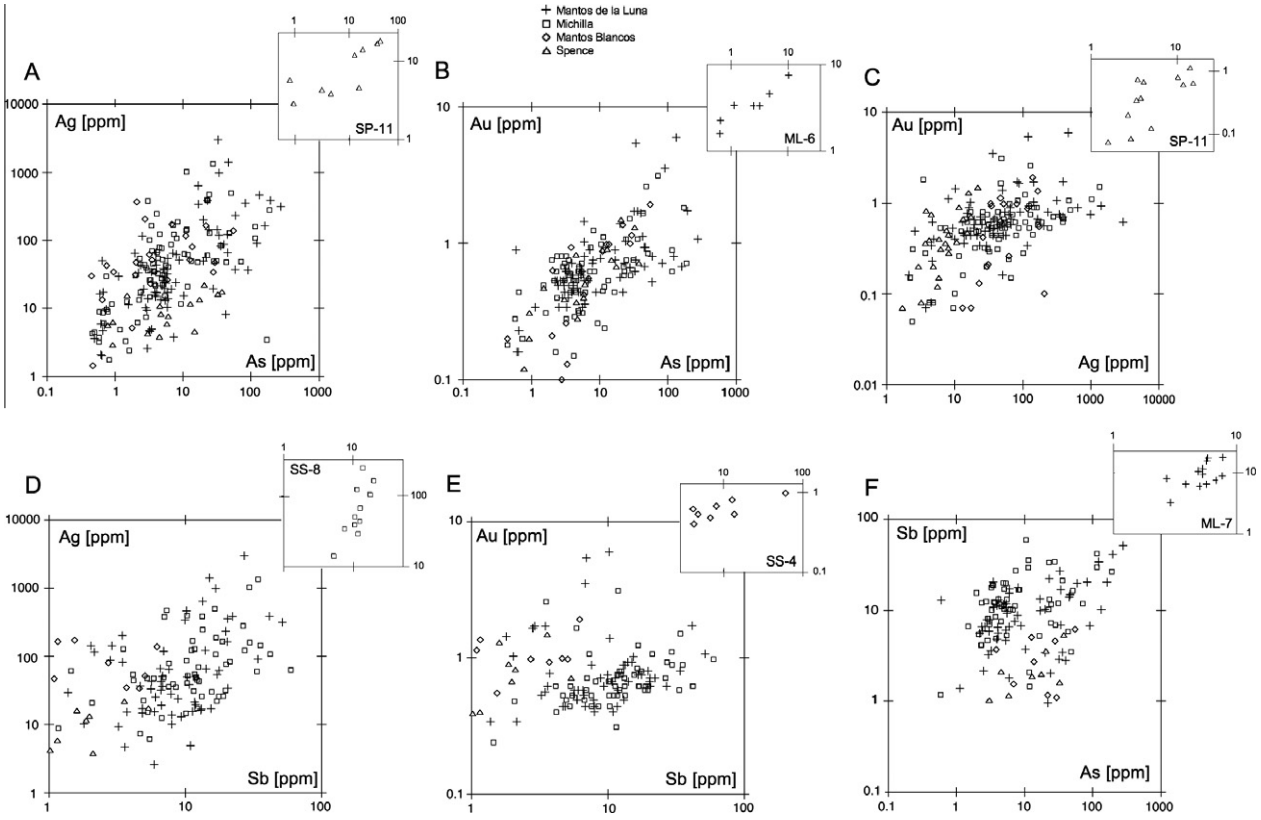

Fig. 2. Correlation plots of (A) Ag *vs.* As, (B) Au *vs.* As, (C) Ag *vs.* Au, (D) Ag *vs.* Sb, (E) Au *vs.* Sb, and (F) Sb *vs.* As. Insets show individual correlations of representative samples. Full SIMS data in Appendix A.

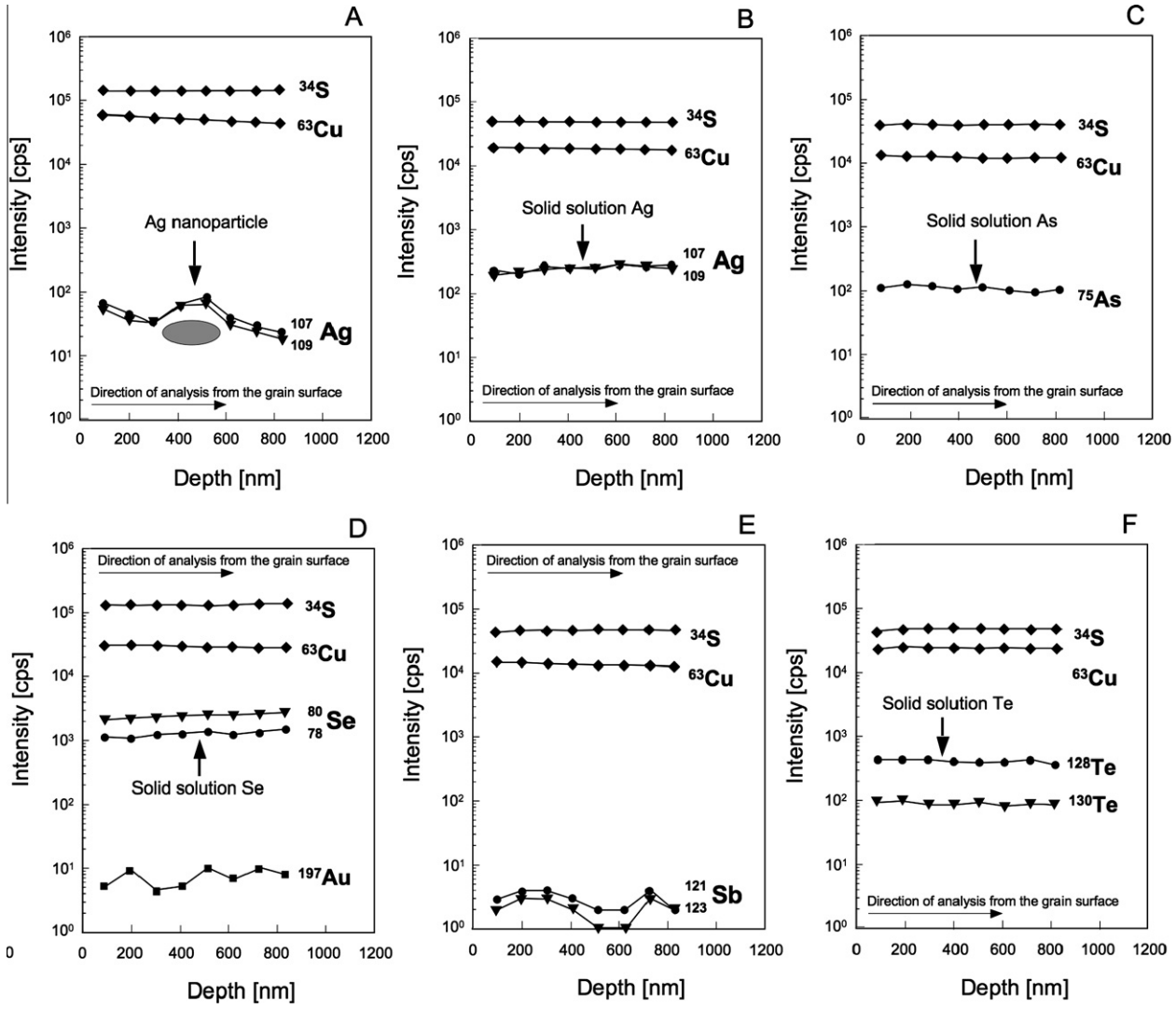

Fig. 3. SIMS depth-concentration profiles (times *vs.* intensity) of trace elements in selected digenite samples: (A) ^{107,109}Ag, sample SP-13 (Spence); (B) ^{107,109}Ag, sample ML-5 (Mantos de la Luna); (C) ^{75}As, sample SS-4 (Michilla); (D) ^{78,80}Se and ^{197}Au, sample SP-11 (Spence); (E) ^{121,123}Sb, sample ML-7 (Mantos de la Luna); (F) ^{130}Te, sample ML-3 (Mantos de la Luna). For each profile, ^{63}Cu and ^{34}S (Cu-sulfide matrix) are shown. Intensity scale in counts per seconds (cps) and depth in nanometers (nm).

nanoparticles smaller than ~50–100 nm. Therefore, TEM observations were performed in representative samples with high Ag/As ratios (>~30). TEM selected area electron diffraction (SAED) patterns of the Cu-sulfide matrix are consistent with the low-digenite structure (cubic, space group $Fd3m$, $a = 5.57$ Å) (Fig. 1B). Fig. 4A–D shows high-resolution TEM images of a selected digenite sample from the Mantos Blancos deposit (MB-14) that plot above the wedge in a Ag *vs.* As plot (369 ppm Ag and 2 ppm As, Figs. 2 and 5, Appendix Table). The conventional TEM images of this anomalous, high-Ag low-As sample (Fig. 4A and B), reveals the presence of discrete, sub-micron sized particles that are disseminated in the digenite matrix. High-magnification TEM images (4×10^6 times) show that the nanoparticles are rounded in shape and range in size between 5 and 10 nm (Fig. 4C and D). Indexing of the two-dimensional lattice fringes of the fast Fourier transformation (FFT) of the TEM images reveals a FCC structure with interplanar spacing consistent with the native silver (Ag^0) structure (inset, Fig. 4C).

4. DISCUSSION

4.1. Mineralogical form of Ag and Au: solid solution *vs.* nanoparticulate

The first database on trace metals (Ag, Au, As, Sb, Se, Te) in supergene Cu-sulfides from various Cu deposits, presented here, reveals that trace-to-minor amounts of Ag and Au are incorporated in digenite as a function of the As content. When the SIMS, EMPA and TEM compositional and mineralogical data for Ag and As are plotted together in a log(Au)–log(As) diagram, it is observed that the datapoints form a wedge-shaped zone with an upper limit that separates

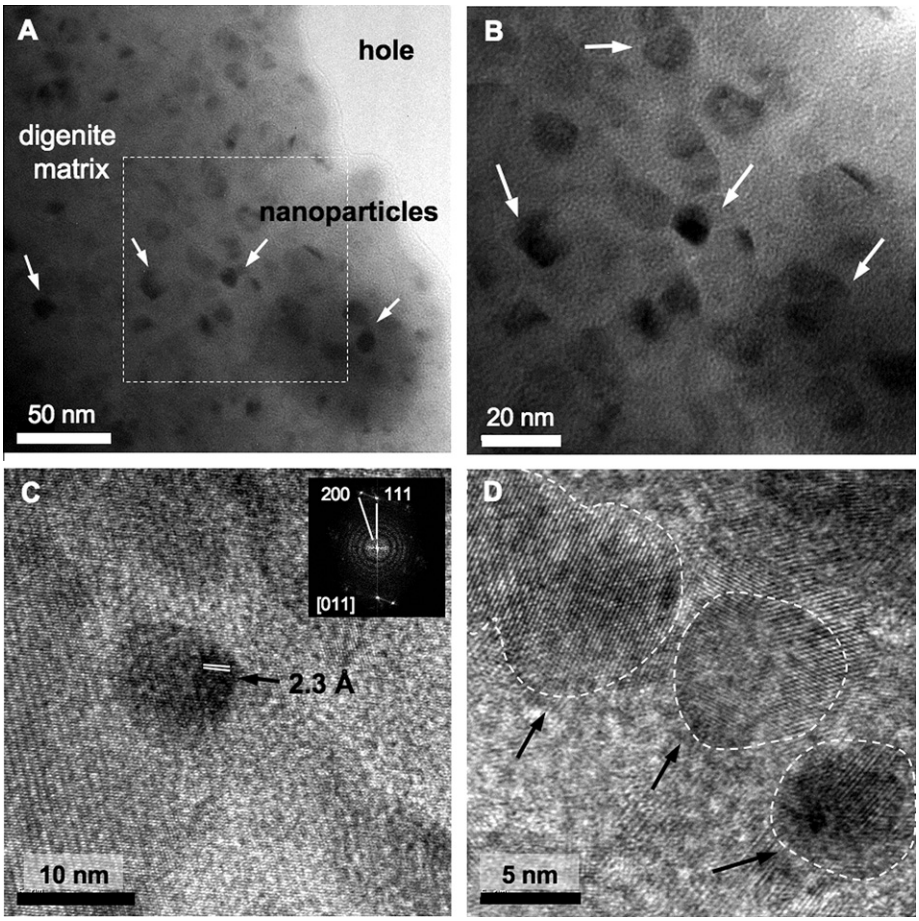

Fig. 4. TEM images of digenite sample MB-14. The selected sample has a high Ag/As ratio and plots above the upper limit in a log(Ag)–log(Au) plot (Fig. 5A). Conventional TEM images (A and B) show the presence of discrete, sub-micron sized particles in the digenite matrix. High-resolution TEM images (C and D) show that the nanoparticles are rounded in shape and range in size between 5 and 10 nm. Inset in (C) is the fast Fourier transformation (FFT) image of a single nanoparticle, suggesting metallic silver (Ag^0) structure.

samples with high and low Ag/As ratios (>~30, and <~30, respectively) (Fig. 5A). The high Ag/As samples plotting above the "wedge" zone (Fig. 5A), contain Ag particles as detected by SIMS depth profiling and TEM observations (samples SP-13 and MB-14, Figs. 3A and 4A–D, respectively). These anomalous, high Ag/As samples show vertical patterns (e.g. ML-1, EMPA/SIMS data) and escape the general correlation trend. In contrast, samples with lower Ag/As ratios plot within the "wedge" zone in the Ag–As plot and show well-defined positive Ag–As correlations (Figs. 5A and 2A, inset). In these samples, SIMS depth profiling reveal that Ag is contained in solid solution (sample ML-5, Fig. 3B). Therefore, the data suggest that Ag occurs in two mineralogical forms in digenite (nanoparticulate and/or solid solution) and that their occurrence is strongly dependent on the contained amount of As (Fig. 5A).

A similar wedge-shaped zone is observed for Au and As in digenite (Figs. 2B and 5B). Low Au/As (<~0.03) samples show positive correlations between the two elements (e.g. Fig. 2B, inset) and SIMS depth profiling suggest that Au is present in solid solution inside the wedge zone (sample SP-11, Fig. 3D). Due to the low concentrations of Au in the samples, the presence of nanoparticulate phases (e.g. Au^0 nanoparticles, Palenik et al., 2004; Reich et al., 2005, 2006) could not be confirmed (nor discarded) for high Au/As samples plotting above the "wedge". Therefore, it is assumed that most of the Au in digenite is contained in solid solution.

Hannington et al. (1988) reported secondary enrichment of Ag and Au in recent submarine sulfides in the TAG hydrothermal field in the rift valley of the Mid-Atlantic Ridge. In these deposits, digenite is the principal secondary Cu-sulfide and replaces chalcopyrite along fractures within grains and around the margins of the Cu–Fe sulfides. Secondary digenites contain an average of 80.6 ppm Ag, 11.2 ppm Au and 54 ppm As. Two mineralogical forms of incorporation of Ag and Au in digenite samples were reported: solid solution and free micro-particles of native Au (<15 μm) (Hannington et al., 1988). When plotted together with the Ag–Au–As data presented in this study, selected TAG digenite samples from Hannington et al. (1988) follow the same behavior reported for digenites in this study. TAG digenite samples containing Ag in solid solution plot inside the wedge zone in the Ag–As plot (Fig. 5A), while samples containing free Au particles plot above the wedge zone in the Au–As plot (Fig. 5B).

4.2. Solubility of Ag and Au in supergene digenite

It is remarkable that the correlations between "invisible" precious metals (Ag, Au) and As in supergene digenite from Cu deposits are comparable with those reported for "invisible" Au in As-rich pyrites from Carlin-type, epithermal and orogenic Au deposits (Wells and Mullens, 1973; Cook and Chryssoulis, 1990; Fleet and Mumin, 1997; Reich et al., 2005; Sung et al., 2009). Gold and As contents in pyrite plot in a wedge-shaped zone bounded by a line that defines the relation between concentrations of Au and As in arsenian pyrite (Reich et al., 2005). Microanalytical results reported by Reich et al. (2005) (SIMS, TEM, XANES–EXAFS) confirmed that arsenian pyrite compositions plotting above the solubility limit contain nanoparticles of native gold (Au^0), whereas compositions plotting below the limit contain Au in solid solution (Au^{1+}). Ciobanu et al. (2009) noted a similar wedge-shaped correlation between Au and Ag in bismuth chalcogenides, and Au concentrations above 100 ppm were reported to be all associated with higher Ag contents.

We propose that the incorporation of Ag and Au in supergene digenite is strongly dependent on the As content, and that the upper limit of the wedge-shaped zones in Fig. 5A and B represent chemical limits of incorporation of precious metals as a function of As. For Ag and Au, the upper limits can be approximated by the lines

$$C_{Ag} = 29.3 \cdot C_{As} + 6.80, \quad \text{and}$$
$$C_{Au} = 0.03 \cdot C_{As} + 0.69 \qquad (3)$$

where C_{Ag}, C_{Au} and C_{As} represent the concentrations of the trace elements in parts per million weight (ppm). These upper limits represent the empirical maximum contents of Ag and Au in supergene digenite as a function of As, and control the occurrence of nanoparticulate *vs.* solid solution (structurally bound) Ag and Au. Based on the available data, we predict that supergene digenite can host three orders of magnitude more Ag (~3000 ppm) than Au (~3 ppm) for the same amount of As (e.g. 100 ppm).

Experimental studies of the solubility of Ag in Au in Cu-sulfides are not currently available at low-temperature, near-surface conditions (i.e. $T < 100$ °C). Above 119 °C, the system Ag_2S–Cu_2S is comprised principally by three $(Ag, Cu)_2S$ complete solid solutions: body-centered cubic (bcc), face-centered cubic (fcc) and hexagonally closed packed (hcp) (Skinner, 1966; Harlov and Sack, 1995). Although direct determination of the solubilities of Ag and Au in low-temperature Cu-sulfides must be addressed experimentally in future studies, the analytical data presented here allows a first-order approximation of the limiting solubility of Ag and Au in supergene digenite.

Our results are in agreement with the very few studies that have reported trace element contents of chalcocite and digenite. Kesler et al. (2002) used SIMS to measure the Au content of Cu–Fe–S and Cu–S sulfides from the Au-rich Batu Hijau, Kingking and Skouries porphyry Cu deposits. Results show that supergene chalcocite (Cu_2S) contain more Au than the Cu–Fe sulfides, with an average of 4.24 ppm Au at Batu Hijau (21 analyses). Although As

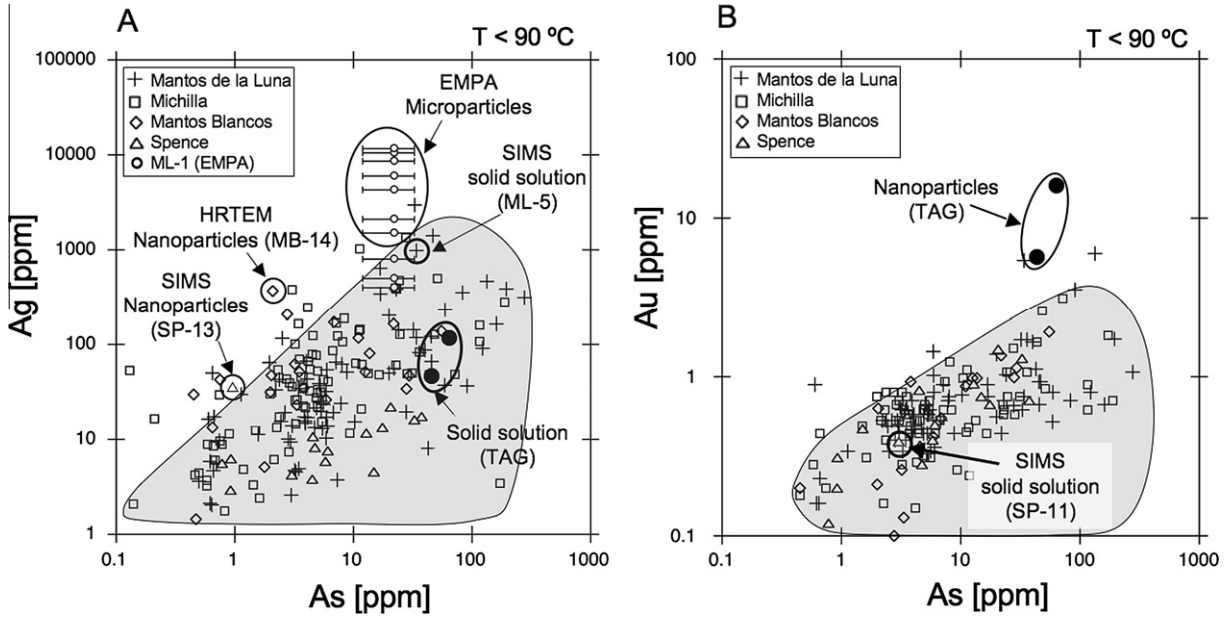

Fig. 5. Ag–As and Au–As plots showing all microanalytical data (SIMS, EMPA, TEM) for supergene digenite. (A) Within the wedge-shaped zone in Ag–As log–log space (shaded), Ag is contained in solid solution as confirmed by SIMS depth profiling. This zone is limited by a line, above which Ag occurs as nanoparticles of metallic Ag (HRTEM, SIMS) and micro- to nano sized particles of Ag iodide (iodargyrite, Reich et al., 2009b). The Ag–As analyses of supergene digenites from massive sulfides (TAG) plot in the solid solution field (Hannington et al., 1988). Horizontal error bars show the compositional range of As in sample ML-1, as measured by SIMS. (B) The Au–As plot (log–log space) shows the solid solution field (shaded, SIMS depth profiling) with a sharp upper limit separating Au in solid solution from Au NPs. Analyses from TAG digenites containing micron-sized native Au particles plot above this limit (Hannington et al., 1988).

nor Ag were reported, nine chalcocite grains contained small (<20 μm) inclusions of native Au. In view of the supergene origin of these chalcocites, the Au is not likely to have exsolved from the sulfides. Instead, it might have been deposited as Au colloid particles during supergene enrichment (Kesler et al., 2002). Clark et al. (2001) used LA-ICP-MS to measure the trace element composition of sulfides at the Mammoth copper deposit in Queensland, Australia, with the aim to distinguish between hypogene and supergene chalcocite. Average concentrations of 32 analyses of supergene chalcocite report Ag and As concentrations of 23 and 7 ppm, respectively, and no Ag inclusions were detected in the analyses (samples plot in the solid solution field of Ag–As plot in Fig. 5A). Recently, Cook et al. (2010) reported LA-ICP-MS analyses of minor elements in primary (hypogene) bornite, chalcocite and digenite from Late Proterozoic vein-type deposits in Scandinavia and from skarn, porphyry and epithermal deposits from the Late Cretaceous Banatitic Magmatic and Metallogenetic Belt of SE of Europe. Results show that Ag and Au are preferentially partitioned into Cu-sulfides (digenite), with Au contents measured up to 24 ppm, supporting the notion that Ag (and probably Ag) concentrates in Cu-sulfides (chalcocite, covellite) rather than bornite.

4.3. Incorporation of trace metals into supergene digenite

Despite its simple composition, the crystal structures of $Cu_{2-x}S$ minerals are very complex. Structure analyses exist for chalcocite, djurleite and anilite (Koto and Morimoto, 1970; Evans, 1979), and recent studies have been published on high and low-digenite and bornite–digenite solid solutions (Grguric and Putnis, 1999; Grguric et al., 2000; Will et al., 2002). Although the phase relations of the Cu-sulfides have been studied extensively at high temperatures, considerable uncertainty exists on the precise temperatures of phase transitions in the very-low-temperature region ($T < 100$ °C). According to Morimoto and Koto (1970) and Morimoto and Gyobu (1971), digenite ($Cu_{1.8}S$) is stable at room temperature only if it contains a small amount of Fe. Digenite can occur as a low-temperature form ("low-digenite", cubic, $a = 5.57$ Å and space group *Fd*3*m*), stable under 91 °C, and a high temperature form, "high-digenite" (cubic, $a = 5.57$–5.64 Å, space group *Fm*3*m*, stable $T > 91$ °C). Both phases are related by a metastable transitional phase which exists between high- and low-digenite around 90 °C (Morimoto and Gyobu, 1971; Will et al., 2002). The EMPA and TEM results presented here are consistent, therefore, with near-ambient formation ($T < 90$ °C) of low-digenite, and support its supergene origin.

The Cu atoms in chalcocite (Cu_2S) structure are highly mobile and are found primarily in triangular coordinations of a disordered cationic substructure (CuS_3 triangles) (Makovicky, 2006; Vaughan and Rosso, 2006). In the absence of spectroscopic information (XPS and XANES/EXAFS analyses usually require thousands of ppm to wt% levels to obtain interpretable spectra) for the studied samples, the substitutional mechanisms of Au, Ag and As in supergene digenite cannot be fully constrained. However, some insights about possible substitutions can be made based on previously published structural data available for Cu-sulfides, including digenite.

Cubic digenite ($Cu_{1.8}S$) exists with a mobile Cu array as in chalcocite, and Cu atoms are coordinated either tetrahedral (Cu^{IV}) and trigonal (Cu^{III}), or all tetrahedral (Pattrick et al., 1997). Harlov and Sack (1995) documented that Ag–Cu substitutions in Ag-poor $(Cu, Ag)_2S$ solid solutions require the involvement of vacancies, due to the fact that these solutions behave as ionic conductors and that Ag^{1+} and Cu^{1+} have different effective ionic radii (0.1 and 0.06 nm, respectively, Shannon, 1976) and stereochemistry. In addition, As (and Sb), Ag and Cu substitutional exchanges are common in sulfosalt fahlores (Ghosal and Sack, 1995; Sack et al., 2005). Therefore, for a predominantly tetrahedral coordination environment for Cu^{1+} in digenite, the coupled substitution $(Ag^{1+}, Au^{1+}) + As^{3+} \Longleftrightarrow 4Cu^{1+}$ is possible as the combined ionic radii of As^{3+} and Ag^{1+} (0.158 nm), and As^{3+} and Au^{1+} (0.195 nm) are in the range of the four Cu ions replaced (0.24 nm).

The same mechanism can be described as $(Ag^{1+}, Au^{1+}) + As^{3+} \Longleftrightarrow (4-x)Cu^{1+} + x\square$, if Cu vacancies (□) are considered. The latter mechanism may be more realistic considering the non-stoichiometric, Cu-deficient nature of supergene digenite. An alternative mechanism may involve the coupled substitution of trivalent Au along with trivalent (or penta-valent) As, with or without Cu vacancies: $Au^{3+} + As^{3+} \Longleftrightarrow (6-x)Cu^{1+} + x\square$; $Au^{3+} + As^{5+} \Longleftrightarrow (8-x)Cu^{1+} + x\square$.

As previously suggested by Reich et al. (2005) and Ciobanu et al. (2009) for pyrite and Bi-chalcogenides, respectively, the incorporation of trace metals in Cu-sulfides might be related to a similar "tuning in" phenomenon allowing the incorporation of a Ag and Au *via* the incorporation of a minor component, in this case As. Arsenic may play a significant role increasing the solubility of Ag and Au in the non-stoichiometric, supergene digenite structure, and at the same time controlling the occurrence of Ag and Au nanoparticles above the solubility limits.

It has been suggested that As coatings in the mineral surface of Fe-sulfide minerals may facilitate the adsorption of Ag and Au complexes by locally causing *p*-type semiconducting properties, giving them a stronger electrochemical interaction with negatively charged ions (Maddox et al., 1998). Recent scanning tunneling microscopy (STM) and synchrotron X-ray photoelectron spectroscopy (SR-XPS) studies have confirmed surface electrochemical potential effects for the accumulation of "invisible" Au and Ag in Cu–Fe–As–S sulfides under hydrothermal conditions (Mikhlin and Romanchenko, 2007). Ab-initio calculations by Reich et al. (2003, 2004) suggested that the defect energy of replacing an Fe atom by a Au atom in pyrite is lowered by ~1 eV if two or more As atoms are in the vicinity. These predictions are confirmed by X-ray absorption near edge structure (XANES) measurements and TEM observations revealing clustering of As atoms in the nearby vicinity of Au nanoparticles and Au-rich zones in sulfidic matrices (Savage et al., 2000; McClenaghan et al., 2004; Palenik et al., 2004). Barzyk et al. (2002) investigated the products of aqueous Ag and Au cementation on non-stoichiometric sulfide grains ($Cu_{2-x}S$). Scanning electron and atomic force

microscopy (SEM/AFM) observations reveal different surface products including mixed Cu–Ag sulfides, Au sulfides and metallic Au crystallites depending on the nature of the noble metal ad the solution composition (e.g. Barzyk et al., 2002). Although no spectroscopic or theoretical information are available for As in Cu-sulfides, precious metals incorporation may be enhanced and/or catalyzed in the presence of As due to electrochemical effects induced in the non-stoichiometric, structurally defectuous $Cu_{1.8}S$ digenite surface.

4.4. Geologic implications

It is well known that strong enrichment in trace metals, most importantly nickel, cobalt, gold, silver, and platinum-group elements occurs during the formation of laterite deposits (Freyssinet et al., 2005). The degree of enrichment will depend on geomorphology, climatic conditions, weathering rate, physical-chemistry of runoff and groundwater, permeability of the gangue rocks, and the mineralogical composition of the primary source of metals (e.g. sulfides *vs.* oxides).

Meteoric supergene enrichment in northern Chile covered a long period of time extending from 44 Ma, and ended near 14–9 Ma with a step-wise onset of the hyper-arid climate conditions in the region, followed by further enrichment/oxidation dominated by highly saline brines under hyper-arid conditions (Alpers and Brimhall, 1988; Sillitoe and McKee, 1996; Arancibia et al., 2006; Cameron et al., 2008, 2010; Reich et al., 2008, 2009a). After bacterially mediated dissolution of hypogene sulfides (e.g. chalcopyrite) in the studied deposits, Ag and Au might have transported predominantly as chloride complexes ($AgCl_2^-$ and $AuCl_4^-$, pH <4 and Cl >35,000 mg/L) under highly acidic and oxidizing conditions, or as metastable thiosulfate complexes ($Ag(S_2O_3)_2^{3-}$, $Au(S_2O_3)_2^{3-}$) under less oxidizing and near-neutral conditions (Seward, 1976; Welham et al., 1993; Freyssinet et al., 2005; Pal'yanova, 2008). Although chloride complexes will dominate Ag–Au transport, the high I/Cl and Br/Cl ligand ratios reported for groundwaters from Cu deposits in the Atacama Desert (Leybourne and Cameron, 2006) indicate that mixed chloride–iodide–bromide complexes of Ag and Au (e.g. $(Ag, Au)X_n^{1-n}$, with X = I, Br) may be involved in supergene enrichment and that AgI(s) and AgBr(s) may be important solubility-limiting phases (Gammons and Yu, 1997; Reich et al., 2009b). Another potentially important means of Ag and Au mobilization are *via* colloidal and nanoparticulate processes (Willam-Jones et al., 2009). In the southern areas of Western Australia, where the groundwaters are highly saline and acidic, Hough et al. (2008) documented the occurrence of exceptionally pure <200 nm diameter, 6 nm thick nanoparticulate gold plates in supergene profiles developed above Au-quartz veins, indicating nanoscale mobility of Au during weathering.

It is likely that rapid, kinetically controlled precipitation of digenite ($Cu_{1.8}S$) at the redox front may have played a critical role in effective scavenging Ag and associated trace metals from highly saline solutions in the near-surface environment. Studies have shown that microbial fixation of Cu at active enrichment fronts between hypogene Cu-sulfides and secondary Cu-sulfides may be a critical factor controlling the kinetics of supergene enrichment (Sillitoe et al., 1996; Southam and Saunders, 2005). Therefore, As-coated, non-stoichiometric digenite mineral surfaces might effectively incorporate Ag and Au into solid solution, and in some cases, scavenge metal clusters and/or metal nanoparticles from locally saturated colloidal suspensions during supergene reworking and redox cycling.

5. CONCLUSIONS

The first comprehensive database of SIMS, EMPA and TEM analyses of trace metals (Ag, Au, As, Sb, Se, Te) in supergene Cu-sulfides from various Cu deposits reveals that trace-to-minor amounts of Ag and Au are incorporated in supergene digenite as a function of the As content. When the microanalytical data for Ag, Au and As are plotted in log–log diagrams, it is observed that the datapoints form wedge-shaped zones with upper limits that separates samples with high and low Ag/As (>∼30 and <∼30, respectively) and Au/As (>∼0.03 and <∼0.03, respectively) ratios. Samples plotting above the "wedge" zones contain nanoparticles of metallic Ag and Au as detected by SIMS depth profiling and TEM observations, while samples with lower Ag/As and Au/As contain structurally-bound Ag and Au.

The Ag–Au–As relations in supergene digenite are remarkably similar with those reported for "invisible" Au in As-rich pyrites from Carlin-type, epithermal and orogenic Au deposits. This strongly suggests that the incorporation of precious metals in sulfide minerals respond to the incorporation of a minor "tuning in" component, in this case As. Arsenic may play a significant role increasing the solubility of Ag and Au in the non-stoichiometric supergene digenite ($Cu_{1.8}S$) structure, controlling, at the same time, the occurrence of Ag and Au nanoparticles above the chemical limits of solid-solution incorporation.

Considering the fact that supergene copper enrichment processes can be active from tens of millions of years (e.g. Atacama Desert) through progressive weathering of enrichment blankets and multiple stages of Cu recycling (Mathur et al., 2009), we conclude that As-bearing supergene digenite may play a previously unforeseen role in scavenging precious metals from undersaturated (or locally slightly supersaturated) solutions in arid to hyper-arid areas.

ACKNOWLEDGMENTS

This study was funded by the Chilean Science and Technology Fund (CONICYT), FONDECYT Grant #11070088 to Martin Reich. We thank Jorge Pizarro (Compañía Minera Mantos de la Luna), Martin Williams and Mario Sáez (Spence, BHP-Billiton) for providing access to the deposits and logistical assistance during open pit and core sampling. We also thank Anglo American and Antofagasta Minerals for providing us with samples from the Mantos Blancos and Michilla deposits, respectively. We are grateful to Carl Henderson at University of Michigan for his valuable help with EMPA measurements and Christian Nievas at LabTEM, Universidad de Chile for his help with sample preparation and TEM observations. The transmission electron

microscope used in this work was acquired under the Mecesup grant UCH-0205. Finally, we acknowledge Associate Editor D.J. Vaughan and reviewers N.J. Cook, R.M. Hough and C.J. Stanley for their insightful comments and suggestions which greatly improved the manuscript.

APPENDIX A

Secondary ion mass spectrometry (SIMS) analyses of Ag, Au, As, Sb, Se and Te in digenites from various Cu–(Ag) deposits. Textures: coarse-grained (CG), >50 μm; fine-grained (FG), <50 μm. Stars in parenthesis (*) indicate samples (and elements) that were depth-profiled with SIMS.

Deposit/ sample	Mineral/ texture	Ag [ppm]	Au [ppm]	As [ppm]	Sb [ppm]	Se [ppm]	Te [ppm]
Mantos de la Luna							
ML-1	Digenite/ CG	8.29	n.d.	b.d.	n.d.	10.3	1.2
		2.30	n.d.	b.d.	n.d.	10.3	0.63
		36.50	n.d.	b.d.	n.d.	11	1.69
		1.77	n.d.	b.d.	n.d.	11.8	2.1
		2.04	n.d.	0.64	b.d.	11.9	2.01
		17.20	n.d.	0.67	b.d.	9.28	1.6
	Digenite/ FG	50	1.39	20	10.3	4.53	2.7
		202	0.56	20	3.45	8.98	2.7
		56	0.44	22	0.95	7.83	2.33
		143	1.03	24	2.03	9.89	3.41
		464	5.98	134	10.2	3.59	13
		143	1.71	32	2.89	8.85	3.68
		82	1.71	36	3.46	9.15	3.45
ML-3	Digenite/ CG	28.00	0.49	b.d.	7.86	57.1	17.8
		14.80	0.44	3.93	4.84	50.9	16.6 (*)
		91.10	0.80	123	34	44.6	14.7
		33.30	0.53	2.22	5.59	54.7	10.5
		2.60	0.49	2.98	5.91	77	16.1
		15.60	0.71	3.91	11.3	66	9.2
		43.30	0.58	4.07	5.64	34.1	14.1
		15.40	0.49	2.45	5.95	64.7	12.1
		13.90	0.44	3.05	7.95	39.6	14.8
		43.00	0.53	2.38	6.63	51.7	14.9
		36.80	0.44	5.24	4.66	91.3	15.8
		19.20	0.53	6.78	b.d.	40.7	17.5
		1417	0.93	46.8	15	29.5	12.8
		19.20	0.53	2.65	6.66	47.8	13.6
		639	0.89	16.77	13.4	24.6	9.5
		16.30	0.89	0.60	13.	50.7	5.06
		119	5.42	33.90	6.93	76.6	9.32
	Digenite/ FG	164	0.67	161	20.3	36.7	14.7
		388	1.73	195	41.4	11.3	15.8
		343	0.75	16.90	9.95	31.6	8.88
		122	0.93	45.30	14	70.3	8.92
ML-4	Digenite/ CG	9.67	n.d.	0.74	n.d.	15.9	1
		3.60	n.d.	b.d.	n.d.	10.8	0.7
		11.90	n.d.	b.d.	n.d.	9.89	2.06
		b.d.	n.d.	1.04	n.d.	12.8	1.23
		37.10	0.52	58.90	b.d.	12.2	2.16
		14.80	n.d.	b.d.	n.d.	11.1	1.91
		5.25	n.d.	b.d.	n.d.	12.6	0.67
		3.33	n.d.	b.d.	n.d.	11.8	0.93
		5.89	n.d.	0.62	n.d.	9.33	2.27
	Digenite/ FG	19.50	0.66	27.90	b.d.	12.2	2.84
		87.70	1.66	40.10	2.81	4.19	2.93
		5.63	n.d.	0.70	b.d.	9.48	1.05
ML-5	Digenite/ CG	385	0.71	23.00	22.2	52.6	9.59
		34.30	0.62	3.45	20.5	85.4	8.79
		17.20	0.44	3.87	4.84	58.2	12.4
		4.93	0.40	3.47	10.9	32.9	11.3
		17.00	0.49	4.11	13.1	58.2	9.37
		21.40	0.44	4.89	11.7	35.3	12.8
		4.71	0.62	3.20	3.6	35.8	9.24
		51.00	0.44	8.82	6.79	28.8	11.2
	Digenite/ FG	66.1	0.67	45.5	14.2	79.5	10
		233	0.80	59.3	19.8	26.3	9.1
		988 (*)	0.75	33.9	16.7	24.4	10.7
		2977	0.62	32.9	27	41.5	9.1
		355	0.71	83	20.4	81.8	10.8
		314	1.07	277	51.4	30.3	17.9
ML-6	Digenite/ CG	50.1	0.16	0.65	b.d.	4.83	2.86
		29.6	0.34	1.13	1.38	6.91	2.45
		116	0.34	2.52	2.15	3.98	2.78
		3.63	n.d.	0.50	b.d.	4.07	0.91
		15.3	0.77	10.24	3.73	4.38	2.06
		4.67	0.23	0.66	n.d.	4.53	2.56
		8.58	n.d.	b.d.	b.d.	4.8	3.24
		b.d.	0.12	b.d.	n.d.	1.82	2.83
		4.56	0.34	3.27	n.d.	5.33	2.6
		13.4	0.47	4.70	b.d.	2.95	2.6
ML-7	Digenite/ CG	9.37	0.53	2.96	3.24	22.5	8.48
		10.10	0.40	2.82	7.95	7.73	9.72
		54.00	0.80	5.95	17.1 (*)	77.9	8.92
		32.00	0.53	5.89	6.62	16.6	13.36
		66.40	0.58	4.00	6.53	14.6	9.5
		17.10	1.02	5.93	15.4	21.3	8.48
		13.10	0.62	5.49	9.32	13.8	7.64
		23.90	0.71	7.84	8.84	16.6	9.32
		65.00	0.89	7.13	7.59	19.5	7.24
		25.40	0.58	5.27	6.04	13.6	8.52
		19.60	0.58	5.35	11.9	11.5	9.19
		62.20	0.75	8	17.7	33.5	7.15
		38.60	0.67	5.13	10.7	17.3	9.24
ML-8	Digenite/ CG	3.85	n.d.	b.d.	n.d.	2.7	2.11
		4.51	0.08	b.d.	n.d.	3.67	2.41
		10	n.d.	b.d.	n.d.	2.88	1.89
		8.6	n.d.	b.d.	n.d.	5.75	0.73
		2.12	0.16	0.62	n.d.	6.38	2.23

Appendix A (*continued*)

Appendix A (*continued*)

Deposit/ sample	Mineral/ texture	Ag [ppm]	Au [ppm]	As [ppm]	Sb [ppm]	Se [ppm]	Te [ppm]
		64.7	b.d.	1.96	n.d.	3.55	1.09
	Digenite/ FG	36.5	3.54	90.8	6.79	4.16	6.58
		8.09	1.12	42.7	b.d.	5.39	3.58
		11.30	n.d.	1.58	b.d.	9.38	3.3
		13.80	0.36	6.06	b.d.	5.44	2.5
		23.40	0.34	5.60	n.d.	6.8	1.87
		10.30	1.44	5.90	1.8	11.3	4.61
		3.76	0.07	7.32	n.d.	5.6	2.38
Michilla (Lince–Estefanía)							
SS-1	Digenite/ CG	4.24	0.08	0.46	n.d.	12.3	2.77
		8.88	n.d.	0.78	n.d.	8.96	1.92
		17.5	n.d.	b.d.	b.d.	14.8	0.75
		2.22	n.d.	b.d.	n.d.	9.7	2.12
		48.50	3.12	71.60	11.9	5.39	4.41
		3.32	n.d.	1.43	n.d.	10.2	0.95
		1.77	n.d.	0.82	n.d.	12.4	2.91
	Digenite/ FG	27.50	0.32	4.85	n.d.	3.79	2.35
		11.60	0.26	9.33	n.d.	9.72	1.67
		32.40	0.29	4.27	b.d.	10.1	2.36
		34.40	n.d.	3.79	n.d.	7.43	1.92
		66.70	0.15	4.17	b.d.	9.1	1.21
SS-2	Digenite/ CG	160	0.89	116	29.7	60.6	13.4
		22.50	0.49	3.78	4.93	90.9	15.3
		25.90	0.71	5.47	13.2	94.3	7.33
		31.60	0.58	5.290	19.7	65.4	7.24
		78.80	0.44	4.51	7.59	34.4	14.1
		17.20	0.80	2.38	12.2	86	10
		35.60	0.44	3.71	8.52	50.5	15.1
		14.60	0.67	3.27	10.1	53.1	5.77
	Digenite/ FG	387	0.62	23.20	13.3	41.4	9.63
		280	0.71	189	26.5	26.8	13.3
		49.10	0.58	28.40	6.93	35.8	8.84
		397	0.67	22.50	10.3	22.2	11.9
		128	0.75	24.60	11.7	44	10
		475	1.07	24.40	7.28	69.9	8.04
SS-3	Digenite/ CG	2.21	0.15	n.d.	n.d.	7.63	2.65
		8.88	n.d.	0.59	1.17	10.2	1.64
		b.d.	n.d.	2.43	n.d.	12	1.96
		5.2	n.d.	b.d.	n.d.	9.72	2.78
		b.d.	n.d.	b.d.	n.d.	10.7	2.41
		3.23	n.d.	0.58	n.d.	9.93	2.11
		2.09	n.d.	0.14	n.d.	10.8	2.19
	Digenite/ FG	13.3	0.16	2.26	b.d.	16.9	1.98
		20.90	0.48	11.7	2.07	19.9	1.77
		47.80	1.66	43.6	5.86	12.8	4.12
		61.50	0.24	11.8	1.45	12.1	2.49
		6.04	n.d.	0.68	b.d.	8.97	0.84
		49.60	0.53	13.40	b.d.	6.46	2.37
SS-4	Digenite/ CG	12.50	0.49	1.5	6.7	31.7	8.3
		44.60	0.40	2.36	4.17	35.7	9.81
		7.37	0.53	2.85	4.66	45.7	8.75

Appendix A (*continued*)

Deposit/ sample	Mineral/ texture	Ag [ppm]	Au [ppm]	As [ppm]	Sb [ppm]	Se [ppm]	Te [ppm]
		63.30	0.98	10.50	59.5	52.1	6.22
		54	0.62	2.31	4.13	26.6	8.17
		39.30	0.67	2.89	8.13	48.3	9.19
		43.30	0.80	2.74	12.6	77.6	5.06
	Digenite/ FG	50.00	0.75	31.30	12	37.4	9.68
		6.15	0.53	2.14	5.46	47.1	9.63
		500	0.84	51.20 (*)	16.4	41.8	7.24
		83.7	1.07	35.90	21.2	34.9	7.55
		47.8	0.44	16.50	5.24	47.2	12.8
		108	0.62	116	41.9	96	12.5
		60.3	0.58	22.9	33.5	29.3	8.97
		1346	1.51	27.7	34.2	43.9	7.46
SS-5	Digenite/ CG	53.5	b.d.	0.13	n.d.	18.9	1.49
		3.46	1.82	173	b.d.	15.6	6.69
		n.d.	n.d.	b.d.	n.d.	10.4	0.83
		16.40	n.d.	0.21	n.d.	11.7	1.84
		2.42	0.31	1.62	n.d.	11.88	3.87
		b.d.	0.07	1.94	n.d.	8.64	2.45
	Digenite/ FG	128	2.6	48.3	3.5	10.3	5
		42.7	0.31	5.61	n.d.	10.4	2.47
		101	0.28	3.23	b.d.	6.93	1.89
		11.5	b.d.	0.9	n.d.	7.11	0.99
		140	0.45	11.2	b.d.	9.42	2.55
		21.6	n.d.	3.93	n.d.	14.1	0.73
SS-6	Digenite/ CG	30.2	0.75	1.98	15.6	9.24	8.21
		22.1	0.62	5	17	17.4	12.5
		1025	1.11	11.3	29.5	28	8.7
		76.6	0.62	4.87	19.9	21.5	14.5
		123	0.93	7.37	27.2	19.1	9.28
		25.9	0.8	3.22	17.6	19.9	12.3
		26.1	0.62	3.36	19	13.6	10.1
		145	0.89	11.4	35.5	23.4	7.95
		168	0.62	7.18	11.3	17.4	8.7
		188	0.62	8.37	16.8	7.8	8.3
		86.4	0.53	6.69	10.2	17.6	13.8
		54.4	0.53	4.31	11.7	11	16.1
SS-8	Digenite/ CG	246	0.53	4.11	13.4	12.4	10.5
		165	0.58	3.45	18.7	16	13
		45.4	0.58	3.62	12.2	12.5	9.81
		36.1	0.53	3.05	7.55	20.8	13.9
		381	0.71	3.05	7.02	15.8	16.7
		31	0.31	4.98	11.5	11.3	14.3
		107	1.24	8.11	16.7	25.4	9.41
		69.8	0.75	3.51	12.5	18.9	7.86
		124	0.53	4.56	11.1	19.8	15.4
		52.2	0.67	4.98	10.4	14.2	11.3
		40.7	0.44	6.13	10.3	23.1	15.1
		15.3	0.62	5.4	5.3	20.6	14.8
SS-9	Digenite/ CG	20	0.32	b.d.	n.d.	4.76	1.13
		2.66	n.d.	b.d.	n.d.	3.83	2.12
		4.83	0.08	1.18	b.d.	4.05	1.67

(*continued on next page*)

Appendix A (*continued*)

Deposit/ sample	Mineral/ texture	Ag [ppm]	Au [ppm]	As [ppm]	Sb [ppm]	Se [ppm]	Te [ppm]
		8.54	0.44	0.66	n.d.	4.09	1.83
		29.5	0.2	0.74	b.d.	5.68	1.75
		b.d.	0.18	0.45	n.d.	2.53	1.39
		3.73	0.28	0.58	n.d.	4.37	0.58
		4.44	n.d.	0.5	n.d.	7.56	2.06
		9.61	0.07	0.75	n.d.	2.61	0.7
		10.1	0.1	b.d.	n.d.	4.42	0.81
		2.38	0.05	b.d.	n.d.	4.05	0.92
Mantos Blancos							
MB-14	Digenite/ CG	b.d.	n.d.	b.d.	n.d.	13.3	0.75
		13.6	n.d.	b.d.	n.d.	9.15	1.81
		7.16	n.d.	b.d.	n.d.	17.6	1.98
		29.8	0.2	0.45	n.d.	12.7	0.99
		5.1	n.d.	1.78	n.d.	14.8	2.08
		1.97	n.d.	b.d.	n.d.	13.5	0.82
	Digenite/ FG	26.1	0.42	5.91	b.d.	9.26	1.93
		80.6	0.98	13.7	2.72	7.29	2.61
		34.3	n.d.	0.95	n.d.	9.63	1.75
		51.4	n.d.	3.5	n.d.	9.62	1.97
		369	n.d.	2.09	b.d.	7.35	1.67
		139	1.92	55.3	6.2	6.51	6.41
		165	1.36	21.8	1.16	3.55	3.17
		207	0.1	2.76	b.d.	11.9	2.3
MB-16	Digenite/ CG	17.5	0.07	b.d.	n.d.	8.46	3.14
		13.1	0.07	b.d.	n.d.	8.39	2.65
		9.13	n.d.	b.d.	b.d.	9.01	2.2
		6.95	n.d.	b.d.	n.d.	10	3.26
		104	n.d.	b.d.	n.d.	14.7	0.97
		7.78	n.d.	b.d.	n.d.	17.3	0.75
		13.4	n.d.	0.65	n.d.	7.45	1.78
	Digenite/ FG	34.8	0.93	3.81	3.7	8.63	2.07
		31.3	0.21	2	b.d.	12.7	1.84
		47.3	0.63	2.03	b.d.	2.79	2.66
		51.7	0.98	12.6	5.07	9.47	2.15
MB-22	Digenite/ CG	b.d.	n.d.	b.d.	n.d.	9.78	0.63
		14.1	b.d.	b.d.	b.d.	11.6	1.65
		22.8	n.d.	b.d.	n.d.	9.04	2.18
		42.5	n.d.	0.75	n.d.	11	1.5
		1.45	n.d.	0.47	n.d.	8.06	1.49
		b.d.	n.d.	b.d.	n.d.	11	2.61
		34	0.99	28.1	4.6	10.3	2.74
		172	0.55	6.85	1.54	7.76	1.71
	Digenite/ FG	23	0.13	3.34	b.d.	9.6	2.62
		117	0.87	11	b.d.	7.26	2.17
		62	0.26	3.21	b.d.	8.35	1.82
		47	1.14	29.6	1.09	11.9	3
Spence							
SP-11	Digenite/ CG	3.82	0.82	4.5	2.1	6.8	2.63
		3.73	0.36	b.d.	b.d.	5.98	2.09
		1.7	0.07	b.d.	n.d.	5.62	1.91
		2.22	b.d.	b.d.	b.d.	9.45	2.27
		4.22	0.39 (*)	3.03	1.02	16.6 (*)	1.66
		3.22	0.08	b.d.	n.d.	5.88	1.72
		17.4	0.71	37.5	5.36	6.55	7.59
		13.4	0.67	17.6	1.98	10.7	4.93
		4.53	0.75	14.9	b.d.	8.65	2.38
		5.59	0.12	0.78	b.d.	11.4	1.71
		16.1	1.3	32.7	1.6	6.02	3.41
		11.6	0.9	12.8	1.87	5.15	2.51
		2.93	0.2	0.92	n.d.	6.68	1.78
SP-13	Digenite/ CG	4.87	0.20	b.d.	n.d.	5.88	2.2
		5.87	0.15	b.d.	n.d.	8.04	2.03
		7.29	0.36	b.d.	n.d.	5.73	2.67
		7.60	0.50	6.09	n.d.	5.82	2.46
		8.10	0.32	b.d.	n.d.	6.16	1.68
		8.13	0.45	b.d.	n.d.	6.76	1.67
		6.23	0.31	0.93	b.d.	5.89	2.470
	Digenite/ FG	10.70	0.37	4.56	n.d.	5.97	1.83
		8.22	0.28	4.72	n.d.	15.5	1.91
		21.90	1.49	20.70	3.57	10.7	2.42
		34.0 (*)	1.1	0.95	b.d.	7.83	2.65
		5.88	0.40	5.82	1.15	7.36	2.11

REFERENCES

Ague J. J. and Brimhall G. H. (1989) Geochemical modeling of steady state fluid flow and chemical reaction during supergene enrichment of porphyry copper deposits. *Econ. Geol.* **84**, 506–528.

Alpers C. N. and Brimhall G. H. (1988) Middle Miocene climatic change in the Atacama Desert, northern Chile: evidence from supergene mineralization at La Escondida. *Geol. Soc. Am. Bull.* **100**, 1640–1656.

Arancibia G., Matthews S. J. and De Arce C. P. (2006) K–Ar and Ar-40/Ar-39 geochronology of supergene processes in the Atacama Desert, Northern Chile: tectonic and climatic relations. *J. Geol. Soc. Lond.* **163**, 107–118.

Arehart G. B., Chryssoulis S. L. and Kesler S. E. (1993) Gold and arsenic in iron sulfides from sediment-hosted disseminated gold deposits: implications for depositional processes. *Econ. Geol.* **88**, 171–185.

Barzyk W., Kowal A. and Pomianowski A. (2002) Noble metal (Ag, Au) cementation on non-stoichiometric cuprous sulphide grains. *Colloids Surf.* **208**, 321–335.

Belogub E. V., Novoselov K. A., Yakovleva V. A. and Spiro B. (2008) Supergene sulphides and related minerals in supergene profiles of VHMS deposits from the South Urals. *Ore Geol. Rev.* **33**, 239–254.

Bowles J. F. W. (1986) The development of platinum-group minerals in laterites. *Econ. Geol.* **81**, 1276–1285.

Boyle D. R. (1997) Iodargyrite as an indicator of arid climatic conditions and its association with gold-bearing glacial tills of the Chibougamau–Chapais area, Quebec. *Can. Mineral.* **35**, 23–34.

Brimhall G. H., Alpers C. N. and Cunningham A. B. (1985) Analysis of supergene ore-forming processes and ground-water solute transport using mass balance principles. *Econ. Geol.* **80**, 1227–1256.

Cameron E. M., Leybourne M. I. and Palacios C. (2007) Atacamite in the oxide zone of copper deposits in northern Chile: involvement of deep formation waters? *Miner. Deposita* **42**, 205–218.

Cameron E. M., Leybourne M. I., Palacios C. and Reich M. (2008) Geochemical exploration and metallogenic studies, Northern Chile. *Geosci. Can.* **35**, 97–107.

Cameron E. M., Leybourne M. I., Reich M. and Palacios C. (2010) Geochemical anomalies in northern Chile as a surface expression of the extended supergene metallogenesis of buried copper deposits. *Geochem. Explor. Environ. Anal.* **10**, 1–14.

Chryssoulis S. (1990) Detection and quantification of "invisible" gold by microprobe techniques. In *Proc. Symp. Gold 90', Soc. for Mining, Metall., and Explor.* (eds. D. M. Hausen, D. N. Halbe, E. U. Petersen and W. J. Tafuri). Littleton, pp. 323–331.

Chryssoulis S. L., Cabri L. J. and Salter R. S. (1987) Direct determination of invisible gold in refractory sulphide ores. In *Proc. Internat. Symp. On Gold Metallurgy-Refract. Gold* (eds. R. S. Salter, D. M. Wyslouzil and G. W. McDonald). Pergamon Press, pp. 235–244.

Chryssoulis S. L., Dunne R. and Coetzee A. (2004) Diagnostic microbeam technology in gold ore processing. *J. Miner. Met. Mater. Soc.* **56**, 53–57.

Ciobanu C. L., Cook N. J., Pring A., Brugger J., Danyushevsky L. V. and Shimizu M. (2009) "Invisible gold" in bismuth chalcogenides. *Geochim. Cosmochim. Acta* **73**, 1970–1999.

Clark D. J., Gemmell J. B., Norman M., and Hespe A. M. (2001) Textural and geochemical distinction between supergene and hypogene Cu sulfide phases at the Mammoth copper deposit, Queensland, Australia. Mineral Deposits at the Beginning of the 21st Century. In *Proceedings of the 6th Biennal SGA-SEG Meeting*, (eds. Piestrzyński et al.), Warsaw, Poland, pp. 219–222.

Clarke J. D. A. (2006) Antiquity of aridity in the Chilean Atacama Desert. *Geomorphology* **73**, 101–114.

Colin F., Sanfo Z., Brown E., Bourles D. and Minko A. E. (1997) Gold: a tracer of the dynamics of tropical laterites. *Geology* **25**, 81–84.

Cook N. J. and Chryssoulis S. L. (1990) Concentrations of invisible gold in the common sulfides. *Can. Mineral.* **28**, 1–16.

Cook N. J., Ciobanu C. L., Danyushevsky L. V., and Gilbert S. (2010) LA-ICP-MS analysis of minor elements in bornite, chalcocite and digenite. In *Proceedings, 13th IAGOD Symposium, Adelaide*, Australia, 9–12 April 2010, pp. 199–200.

De Ronde C. E. J., Hannington M. D., Stoffers P., Wright I. C., Ditchburn R. G., Reyes A. G., Baker E. T., Massoth G. J., Lupton J. E., Walker S. L., Greene R. R., Soong C. W. R., Ishibashi J., Lebon G. T., Bray C. J. and Resing J. A. (2005) Evolution of a submarine magmatic–hydrothermal system: brothers volcano, southern Karmadec arc, New Zealand. *Econ. Geol.* **100**, 1097–1133.

Enders M. S., Knickerbockr C., Titley S. R. and Southam G. (2006) The role of bacteria in the supergene environment of the Morenci porphyry copper deposit, Greenlee County, Arizona. *Econ. Geol.* **101**, 59–70.

Evans, Jr., H. T. (1979) The crystal structures of low chalcocite and djurleite. *Z. Kristallogr.* **150**, 299–320.

Fleet M. E. (2006) Phase equilibria at high temperatures. *Rev. Mineral. Geochem.* **61**, 365–419.

Fleet M. E. and Mumin A. H. (1997) Gold-bearing arsenian pyrite and marcasite and arsenopyrite from Carlin Trend gold deposits and laboratory synthesis. *Am. Mineral.* **82**, 182–193.

Freyssinet P., Zeegers H. and Tardy Y. (1989) Morphology and geochemistry of gold grains in lateritic profiles of southern Mali. *J. Geochem. Explor.* **32**, 17–31.

Freyssinet P., Butt C. R. M., Morris R. C., and Piantone P. (2005) Ore-forming processes related to lateritic weathering. In *Economic Geology 100th Anniversary Volume* (eds. J. W. Hedenquist, J. F. H. Thompson, R. J. Goldfarb and J. P. Richards). Society of Economic Geologists, pp. 681–722.

Gammons C. H. and Yu Y. (1997) The stability of aqueous silver bromide and iodide complexes at 25–300 °C: experiments, theory and geologic applications. *Chem. Geol.* **137**, 155–173.

Ghosal S. and Sack R. O. (1995) As–Sb energetics in argentian sulfosalts. *Geochim. Cosmochim. Acta* **59**, 3573–3579.

Golightly J. P. (1981) Nickeliferous laterite deposits. *Econ. Geol.* **75th Anniv.**, 710–735.

Grguric B. A. and Putnis A. (1999) Rapid exsolution behavior in the bornite–digenite series, and implications for natural ore assemblages. *Miner. Mag.* **63**, 1–12.

Grguric B. A., Harrison R. J. and Putnis A. (2000) Revised phase diagram for the bornite–digenite join from in situ neutron diffraction and DSC experiments. *Miner. Mag.* **64**, 213–231.

Hannington M. D., Thompson G., Rona P. A. and Scott S. D. (1988) Gold and native copper in supergene sulfides from the Mid-Atlantic Ridge. *Nature* **333**, 64–66.

Harlov D. D. and Sack S. O. (1995) Thermochemistry of Ag_2S–Cu_2S sulfide solutions: constraints derived from coexisting Sb_2S_3-bearing sulfosalts. *Geochim. Cosmochim. Acta* **59**, 4351–4365.

Hochella M. F., Moore J. N., Golla U. and Putnis A. (1999) TEM study of samples from acid mine drainage systems: metal–mineral association with implications for transport. *Geochim. Cosmochim. Acta* **63**, 3395–3406.

Hough R. M., Noble R. R. P., Hitchen G. J., Hart R., Reddy S. M., Saunders M., Clode P., Vaughan D., Lowe J., Gray D. J., Anand R. R., Butt C. R. M. and Verral M. (2008) Naturally occurring gold nanoparticles and nanoplates. *Geology* **36**, 571–574.

Kesler S. E., Chryssoulis S. L. and Simon G. (2002) Gold in porphyry copper deposits: its abundance and fate. *Ore Geol. Rev.* **21**, 103–124.

Kimball B. A., Callender E. and Axtmann E. V. (1995) Effects of colloids on metal transport in a river receiving acid-mine drainage, upper Arkansas river, Colorado, USA. *Appl. Geochem.* **10**, 285–306.

Kimball B. E., Mathur R., Dohnalkova A. C., Wall A. J., Runkel R. L. and Brantley S. L. (2009) Copper isotope fractionation in acid mine drainage. *Geochim. Cosmochim. Acta* **73**, 1247–1263.

Kojima S., Astudillo J., Rojo J., Trista D. and Hayashi K. (2003) Ore mineralogy, fluid inclusion, and stable isotopic characteristics of stratiform copper deposits in the coastal Cordillera of northern Chile. *Miner. Deposita* **38**, 208–216.

Koto K. and Morimoto N. (1970) The crystal structure of anilite. *Acta Crystallogr.* **26**, 915–924.

Large D. J., MacQuaker J., Vaughan D. J., Sawlowicz Z. and Gize A. P. (1995) Evidence for low-temperature alteration of sulfides in the Kupferschiefer copper deposits of southwestern Poland. *Econ. Geol.* **90**, 2143–2155.

Larocque A. C. L., Hodgson C. J., Cabri L. J. and Jackman J. A. (1995a) Ion-microprobe analysis of pyrite, chalcopyrite and pyrrhotite from the Mobrun VMS deposit in northwestern Quebec: evidence for metamorphic remobilization of gold. *Can. Mineral.* **33**, 373–388.

Larocque A. C. L., Jackman J. A., Cabri L. J. and Hodgson C. J. (1995b) Calibration of the ion microprobe for the determination of silver in pyrite and chalcopyrite from the Mobrun VMS deposit, Rouyn-Noranda, Quebec. *Can. Mineral.* **33**, 361–372.

Leybourne M. I. and Cameron E. M. (2006) Composition of groundwaters associated with porphyry-Cu deposits, Atacama Desert, Chile: elemental and isotopic constraints on water

sources and water-rock reactions. *Geochim. Cosmochim. Acta* **70**, 1616–1635.

Lichtner P. C. and Biino G. G. (1992) A first principles approach to supergene enrichment of a porphyry copper protore: I. Cu–Fe–S subsystem. *Geochim. Cosmochim. Acta* **56**, 3987–4013.

Maddox L. M., Bancroft G. M., Scaini M. J. and Lorimer J. W. (1998) Invisible gold; comparison of Au deposition on pyrite and arsenopyrite. *Am. Mineral.* **83**, 1240–1245.

Makovicky E. (2006) Crystal structures of sulfides and other chalcogenides. *Rev. Miner. Geochem.* **61**, 7–125.

Maksaev V., Townley B., Palacios C. and Camus F. (2007) Metallic ore deposits. In *The Geology of Chile* (eds. T. Moreno and W. Gibbons). The Geological Society, London, pp. 179–199.

Martycak K., Zeman J. and Vacekvesely M. (1994) Supergene processes on ore-deposits – a source of heavy metals. *Environ. Geol.* **23**, 156–165.

Mathur R., Ruiz J., Titley S., Liermann L., Buss H. and Brantley S. (2005) Cu isotopic fractionation in the supergene environment with and without bacteria. *Geochim. Cosmochim. Acta* **69**, 5233–5246.

Mathur R., Titley S., Barra F., Brantley S., Wilson M., Phillips A., Munizaga F., Maksaev V., Vervoort J. and Hart G. (2009) Exploration potential of Cu isotope fractionation in Porphyry Copper deposits. *J. Geochem. Explor.* **102**, 1–6.

Matlock M. M., Howerton B. S. and Atwood D. A. (2002) Chemical precipitation of heavy metals from acid mine drainage. *Water Res.* **36**, 4757–4764.

McClenaghan S. H., Lentz D. R. and Cabri L. J. (2004) Abundance and speciation of gold in massive sulfide of the Bathrust mining camp, New Brunswick, Canada. *Can. Mineral.* **42**, 851–871.

Mikhlin Y. L. and Romanchenko A. S. (2007) Gold deposition on pyrite and the common sulfide minerals: an STM/STS and SR-XPS study of surface reactions and Au nanoparticles. *Geochim. Cosmochim. Acta* **71**, 5985–6001.

Morimoto N. and Gyobu A. (1971) Composition and stability of digenite. *Am. Mineral.* **56**, 1889–1909.

Morimoto N. and Koto K. (1970) Phase relations of the Cu–S system at low temperatures: stability of anilite. *Am. Mineral.* **55**, 106–117.

Mozgova N. N., Trubkin N. V., Borodaev Y. S., Cherkashev G. A., Stepanova T. V., Semkova T. A. and Upenskaya T. Y. (2008) Mineralogy of massive sulfides from the Ashadze hydrothermal field, 13°N, Mid-Atlantic Ridge. *Can. Mineral.* **46**, 545–567.

Orrego M., Urrutia J., Sanhueza A., Boric R., and Cornejo P. (2006) Mineralización tipo Ox Fe–Cu–Au (IOCG) en el Distrito Mantos Blancos (Cu–Ag), Antofagasta, Norte de Chile. In *Proceedings of the XI Congreso Geológico Chileno*, vol. 2, pp. 331–334.

Palenik C. S., Utsunomiya S., Reich M., Kesler S. E. and Ewing R. C. (2004) "Invisible" gold revealed: direct imaging of gold nanoparticles in a Carlin-type deposit. *Am. Mineral.* **89**, 1359–1366.

Pal'yanova G. (2008) Physicochemical modeling of the coupled behavior of gold and silver in hydrothermal processes: gold fineness, Au/Ag ratios and their possible implications. *Chem. Geol.* **255**, 399–413.

Pattrick R. A. D., Mosselmans J. F. W., Charnock J. M., England K. E. R., Helz G. R., Garner C. D. and Vaughan D. J. (1997) The structure of amorphous copper sulfide precipitates: an X-ray absorption study. *Geochim. Cosmochim. Acta* **61**, 2023–2036.

Posfai M. and Buseck P. R. (1994) Djurleite, digenite and chalcocite: intergrowths and transformations. *Am. Mineral.* **79**, 308–315.

Ramirez L. E., Palacios C., Townley B., Parada M. A., Sial A. N., Fernandez-Turiel J. L., Gimeno D., Garcia-Valles M. and Lehmann B. (2006) The Mantos Blancos copper deposit: an upper Jurassic breccia-style hydrothermal system in the coastal range of northern Chile. *Miner. Deposita* **41**, 246–258.

Reich M., Palenik C. S., Utsunomiya S., Becker U., Stixrude L., Kesler S. E. and Ewing R. C. (2003) Solubility limit of gold in arsenian pyrite from Carlin-type and epithermal deposits: EMPA, SIMS, HRTEM and quantum mechanical constraints. *Proc. Geol. Soc. Am. Abstr. Prog.* **35**, 358.

Reich M., Becker U., and Kesler S. E. (2004) Quantum-mechanical and Monte Carlo simulations of Fe–As–S solid solution properties and the energetics of Au incorporation into arsenian pyrite. *Geochim. Cosmochim. Acta* **68** (11). In 1*4th Annual Goldschmidt Conference, Copenhagen*, Denmark, June 5–11, pp. A81.

Reich M., Kesler S. E., Utsunomiya S., Palenik C. S., Chryssoulis S. L. and Ewing R. C. (2005) Solubility of gold in arsenian pyrite. *Geochim. Cosmochim. Acta* **69**, 2781–2796.

Reich M., Utsunomiya S., Kesler S. E., Wang L. M., Ewing R. C. and Becker U. (2006) Thermal behavior of metal nanoparticles in geologic materials. *Geology* **34**, 1033–1036.

Reich M., Palacios C., Parada M. A., Fehn U., Cameron E. M., Leybourne M. I. and Zúñiga A. (2008) Atacamite formation by deep saline waters in copper deposits from the Atacama Desert, Chile: evidence from fluid inclusions, groundwater geochemistry, TEM, and 36Cl data. *Miner. Deposita* **43**, 663–675.

Reich M., Palacios C., Vargas G., Luo . S., Cameron E. M., Leybourne M. I., Parada M. A., Zúñiga A. and You C. F. (2009a) Supergene enrichment of copper deposits since the onset of modern hyperaridity in the Atacama Desert, Chile. *Miner. Deposita* **44**, 497–504.

Reich M., Palacios C., Alvear M., Cameron E. M., Leybourne M. I. and Deditius A. (2009b) Iodine-rich waters involved in supergene enrichment of the Mantos de la Luna argentiferous copper deposit, Atacama Desert, Chile. *Miner. Deposita* **44**, 719–722.

Sack R. O. (2000) Internally consistent database for sulfides and sulfosalts in the system Ag_2S–Cu_2S–ZnS–Sb_2S_3–As_2S_3. *Geochim. Cosmochim. Acta* **64**, 3803–3812.

Sack R. O. and Ebel D. S. (2006) Thermochemistry of sulfide mineral solutions. *Rev. Miner. Geochem.* **61**, 265–364.

Sack R. O., Frederick R., Hardy L. S. and Ebel D. S. (2005) Origin of high-Ag fahlores from the Galena Mine, Wallace, Idaho, USA. *Am. Mineral.* **90**, 1000–1007.

Savage K. S., Tingle T. N., O'Day P. A., Waychunas G. A. and Bird D. K. (2000) Arsenic speciation in pyrite and secondary weathering phases, Mother Lode gold district, Tuolumne County, California. *Appl. Geochem.* **15**, 1219–1244.

Seward T. M. (1976) The stability of chloride complexes of silver in hydrothermal solutions up to 350 °C. *Geochim. Cosmochim. Acta* **40**, 1329–1341.

Shannon R. D. (1976) Revised effective ionic radii and systematic studies of interatomic distances in halides and chalcogenides. *Acta Crystallogr.* **A32**, 751–767.

Sillitoe R. H. (2005) Supergene oxidized and enriched porphyry copper and related deposits. *Econ. Geol.* **100th Anniv.**, 723–768.

Sillitoe R. H. and McKee E. H. (1996) Age of supergene oxidation and enrichment in the Chilean porphyry copper province. *Econ. Geol.* **91**, 164–179.

Sillitoe R. H., Folk R. L. and Saric N. (1996) Bacteria as mediators of copper sulfide enrichment during weathering. *Science* **272**, 1153–1155.

Skinner B. J. (1966) The system Cu–Ag–S. *Econ. Geol.* **61**, 1–26.

Southam G. and Saunders J. A. (2005) The geomicrobiology of ore deposits. *Econ. Geol.* **100**, 1067–1084.

Sung Y. H., Brugger J., Ciobanu A., Pring A., Skinner W. and Nugus M. (2009) Invisible gold in arsenian pyrite and arsenopyrite from a multistage Archean gold deposit: sunrise Dam, Eastern Goldfields Province, Western Australia. *Miner. Deposita* **44**, 765–791.

Trista-Aguilera D., Barra F., Ruiz J., Morata D., Talavera-Mendoza O., Kojima S. and Ferraris F. (2006) Re–Os isotope systematics for the Lince–Estefania deposit: constraints on the timing and source of copper mineralization in a stratabound copperdeposit, Coastal Cordillera of Northern Chile. *Miner. Deposita* **41**, 99–105.

Vaughan D. J. and Craig J. R. (1978) *Mineral Chemistry of Metal Sulfides*. Cambridge University Press, Cambridge, London.

Vaughan D. J. and Rosso K. M. (2006) Chemical bonding in sulfide minerals. *Rev. Miner. Geochem.* **61**, 231–264.

Vivallo W. and Henriquez F. (1998) Genesis comun de los yacimientos estratoligados y vetiformes de cobre del Jurasico Medio a Superior en la Cordillera de la Costa, region de Antofagasta, Chile. *Rev. Geol. Chile* **25**, 199–228.

Welham N. J., Kelsall G. H. and Diaz M. A. (1993) Thermodynamics of Ag–Cl–H_2O, Ag–Br–H_2O, and Ag–I–H_2O systems at 298 K. *J. Electroanal. Chem.* **361**, 39–47.

Wells J. D. and Mullens T. E. (1973) Gold-bearing arsenian pyrite determined by microprobe analysis, Cortez and Carlin Gold mines, Nevada. *Econ. Geol.* **68**, 187–201.

Will G., Hinze E. and Abdelrahman A. R. M. (2002) Crystal structure analysis and refinement of digenite, $Cu_{1.8}S$, in the temperature range 20 to 500 °C under controlled sulfur partial pressure. *Eur. J. Mineral.* **14**, 591–598.

Willam-Jones A. E., Bowell R. J. and Migdisov A. A. (2009) Gold in solution. *Elements* **5**, 281–287.

Associate editor: David J. Vaughan